Environ Earth Sci (2017) 76:366
DOI 10.1007/s12665-017-6691-9

ORIGINAL ARTICLE

Evaluation of present-day rainfall simulations over West Africa in CORDEX regional climate models

A. A. Akinsanola[1,2] · K. O. Ogunjobi[2]

Received: 28 September 2016 / Accepted: 3 May 2017

Abstract The objective of this study is to evaluate the ability of seven CORDEX regional climate models (RCMs), driven by ERA-Interim reanalysis dataset to simulate the observed rainfall characteristics over West Africa during the period of 1990–2008. The seasonal climatology, annual rainfall cycles, interannual variability, 850 hPa specific humidity, and wind fields of the RCMs outputs were assessed over a number of spatial scales covering three climatically homogenous subregions (Guinea Coast, Savannah, and Sahel) and the entire West Africa domain. The ability of the RCMs to simulate the response to El Nino and La Nina events were further assessed. Results indicate that the RCMs captured the spatial pattern of rainfall and the three distinctive phases of the West African monsoon reasonably. It is worth noting that RCA and CRCM5 failed to distinctively reproduce the monsoon jump while CCLM, HIRHAM, and REMO largely overestimated the amount of the pre- and the post-monsoon rainfall. The analysis also showed significant biases in individual models depending on the subregion and season under consideration. These biases appear to be linked to the model's failure to resolve convective processes and topography accurately. The majority of the RCMs used were consistent with the ground observation in capturing the dry (wet) conditions associated with the El Nino (La Nina) events. Statistical analysis conclusively revealed that the RCMs performance varies over the subregions and seasons, implying that no single model is best at all time. In general, REGCM3 was found to be the most outstanding of all the RCMs and is therefore recommended for use in rainfall assessment over West Africa.

Keywords CORDEX-Africa · West African monsoon · Climatology · Precipitation characteristics

Introduction

Rainfall distribution over West Africa is evidently critical for many activities such as hydroelectric power generation, water resources monitoring, rain-fed agriculture, drought, and flood forecasting (Omotosho and Abiodun 2007; Parry et al. 2007; Akinsanola and Ogunjobi 2015). Therefore, variations in rainfall amount have strong and direct implications on the populace and overall economic growth of the region. One of the most crucial and dynamic phenomena of the West African climate system is the West Africa Monsoon (WAM) (Sultan et al. 2011; Akinsanola et al. 2015), a phenomenon caused by the seasonal reversal of winds due to differential heating between land and ocean (Sultan and Janicot 2000; Le Barbé et al. 2002). The WAM plays a vital role in producing majority of the annual rainfall in the region (Omotosho and Abiodun 2007). The flow dynamics of the WAM is generally characterized by the intra-annual movement of the intertropical discontinuity (ITD), triggered by the position of the sun, the West Africa Westerly Jet (WAMJ) which is responsible for the transport of moisture inland, as well as the strength and position of the African Easterly Jet (AEJ) and the Tropical Easterly Jet (TEJ) found at about 600–700 and 200 hPa, respectively (Jung and Kunstmann 2007; Sylla et al. 2013; Akinsanola et al. 2015). The combined baroclinic–

✉ A. A. Akinsanola
aakinsano2-c@my.cityu.edu.hk

[1] School of Energy and Environment, City University of Hong Kong, Kowloon Tong, Hong Kong SAR

[2] Department of Meteorology and Climate Science, Federal University of Technology Akure, Akure, Nigeria

Published online: 13 May 2017

barotropic instabilities of the AEJ are responsible for the formation of African Easterly Waves (AEW) (Redelsperger et al. 2002; Burpee 1972). These waves, in turn, trigger the formation of squall lines and mesoscale convective complexes (Fink and Reiner 2003; Fink et al. 2006). The above-mentioned components interact in a complex way to provide the monsoon rainfall (Sultan et al. 2011). Researches have also shown that interannual and interseasonal variability occurs in the WAM, and has being linked to the influence of some global teleconnections and climate forcing, e.g., El Nino–Southern Oscillation (ENSO), North Atlantic Oscillation (NAO), Madden–Julian Oscillation (MJO), and sea surface temperature (Giannini et al. 2003; Lu and Delworth 2005; Vizy and Cook 2001, 2002).

Presently, there is a limitation in providing skillful and accurate predictions of WAM variability and its impacts on the region. Seasonal forecasts based on empirical data are not always successful (Omotosho and Abiodun 2007). This is primarily due to gaps in the knowledge of coupled atmosphere–land–ocean system probably partly arising from a lack of appropriate ground observation datasets, and also because of the complex scale interactions between the atmosphere, biosphere, and hydrosphere, which ultimately determine the nature of the WAM. (Redelsperger et al. 2006). Providing a solution to the identified gap has become a major concern to scientists and policy makers who develop action plans to mitigate and adapt to the impacts of WAM variability and future climate change. Climate models are the fundamental and primary tools for investigating the climate system response to various forcings, making climate predictions from seasonal to decadal timescales and future climate projection (Akinsanola et al. 2015). However, these dynamic models especially the global circulation models (GCMs) are not without their faults, lacking the resolution needed to adequately resolve ocean wave dynamics, which are important for the correct representation of El Nino development. Also, the model physics are incomplete with many processes and feedbacks on the coupled system being left out. As a result of this poor resolution in the GCMs, previous researches have established their unsuitability for weather and impact studies in regions of complex topography such as West Africa. Recently, the use of regional climate models (RCMs) for dynamical downscaling has grown, their resolution has increased, process descriptions have been developed further, new components are added, coordinated ensemble experiments have become more widespread, and they also show quite realistic climate signals when compared to observations (Rummukainen 2010; Flato et al. 2013). These models are integrated into a limited domain and obtain their initial and boundary conditions from global climate models or gridded analysis of observations. In this way, a RCM acts as a zooming device to deliver climate information on regional to local scale. Comprehensive evaluation of regional downscaling is very difficult especially over West Africa; previous and available studies often employ different methods, regions, periods, and observational data for evaluation. Thus, evaluation results are difficult to generalize. The Coordinated Regional Climate Downscaling Experiment (CORDEX) is an initiative that provides a platform for a joint evaluation of model performance, along with a solid scientific basis for impact assessments and other uses of downscaled climate information (Giorgi et al. 2009).

Published work within CORDEX framework, focusing on the present climate especially precipitation assessment over Africa domain, indicates strengths and deficiencies in the state-of-the-art modeling tools. The first set of the present-day CORDEX simulations using ERA-Interim reanalysis at the boundaries has been analyzed in detail (Nikulin et al. 2012), with focus on precipitation climatology. Results from their study showed a large systematic bias in RCM-simulated annual mean precipitation over Africa. Hence, they reported that the multi-model ensemble mean outperformed individual RCMs. Also, Kim et al. (2014) reported that the RCMs show difficulties in replicating precipitation in arid and semiarid regions of Africa, with quasi-systematic wet biases and a poor capability in reproducing the regional annual cycles. Some other similar and or related studies (Paeth et al. 2011; Druyan et al. 2010; Diallo et al. 2012, 2013; Sylla et al. 2013; Gbobaniyi et al. 2013; Klutse et al. 2015; Akinsanola et al. 2015, 2017) also reported that the RCMs performance varied from one model and region to another. However, most of the aforementioned previous work focused solely on the capability of the RCMs to capture the climatological features and characteristics of the WAM. Presently, there is still limited information on: (1) the specific seasons of individual RCMs strength and weakness from a detailed statistical viewpoint; (2) the basic factors responsible for the deficiencies in the RCMs; and (3) the capabilities of the RCMs to simulate the response to El Nino and La Nina events.

Therefore, providing adequate knowledge and information of the capabilities and limitations of these models in capturing the existing and itemized features is a prerequisite before considering climate change simulations over the region. Hence, this study is aimed at evaluating the ability of seven CORDEX RCMs to reproduce rainfall characteristics over West Africa; indicate the seasons of individual RCMs strength and weakness using a detailed statistical approach; investigate the factors responsible for the deficiencies in the RCMs; and also assess the RCMs ability to simulate response to El Nino and La Nina events.

Table 1 List of CORDEX RCMs used and their schemes (Nikulin et al. 2012)

	DMI-HIRHAM5	ICTP-RegCM3	CLMcom-CCLM4.8	MPI-REMO	SMHI-RCA35	UCT-PRECIS	UQAM-CRCM5
Institute running the model	Danmarks, Meteorologiske Institut, Danmark	International Center for Theoritical Physics, Italy	CLM community (www.clmcommunity.eu)	Max Plank Institue, Germany	Sveriges Meteorologiska och Hydrologiska Institut, Sweden	University of Cape Town, South Africa	Universíe du Qúebec‘ a Montŕeal, Canada
Short name	HIRHAM	REGCM3	CCLM	REMO	RCA	PRECIS	CRCM5
Projection resolution	Rotated pole 0.44	Mercator 50 km	Rotated pole 0.44	Rotated pole 0.44	Rotated pole 0.44	Rotated pole 0.44	Rotated pole 0.44
Vertical coordinates/ levels	Hybrid 3.1	Sigma/18	Terrain following/3.5	Hybrid/27	Hybrid/40	Hybrid/19	Rotated pole 0.44
Advection	Semi-Lagrangian	Eulerian	Fifth-order upwind Baldauf and Schulz (2004)	Semi-Lagrangian	Eulerian	Eulerian	Semi-Lagrangian
Time step (s)	600	100	240	240	1200	300	1200
Convective scheme	Tiedtke (1989)	Grell (1993), Fritsch and Chappell (1980)	Tiedtke (1989)	Tiedtke (1989)	Kain and Fritsch (1990, 1993)	Gregory and Rowntree (1990) Gregory and Allen (1991)	Kain and Fritsch (1990) Kuo (1965)
Radiation scheme	Fouquart and Bomel (1980) Mlawer et al. (1997)	Kiehl et al. (1996)	Ritter and Geleyn (1992)	Morcrette et al. (1986) Giorgetta and Wild (1995)	Savijarvi (1990) Sass et al.(1994)	Edwards and Slingo (Edwards and Slingo 1996)	Li and Barker (2005)
Turbulence vertical diffusion	Louis (1979)	Holtslag et al. (1990)	Herzog et al. (2002), Buzzi et al. 2011)	Louis (1979)	Cuxart and Bougeault (Cuxart and Bougeault 2000)	Wilson (1992)	Benoit et al. (1989) Delage (1997)
Cloud microphysics scheme	Tiedtke (1989), Tompkins (2002)	SUBEX Pal et al. (2000)	Doms et al. (Doms et al. 2007) Baldauf and Schulz (2004)	Lohmann and Roeckner (1996)	Rasch and Kristjanson (1998)	Smith (1990)	Sundqvist et al. (1989)
Land surface scheme	Schulz et al. (1998) Hagemann (2002)	BATS1E Dickinson et al. (1993)	TERRA-ML; Doms et al. 2007)	Hagemann (2002) Rechid et al. (2009)	Samulsson et al. (2006)	MOSES2 Essery et al. (2003)	CLASS 3.5, Verseghy (2000)
Latest reference and comments	Christensen et al. (2006)	Pal et al. (2007)	Rockel et al. (2008), Baldauf et al. (2011)	Jacob (2001), Jacob et al. (2007)	Samuelsson et al. (2011)	Jones et al. (2004)	Zadra et al. (2008)

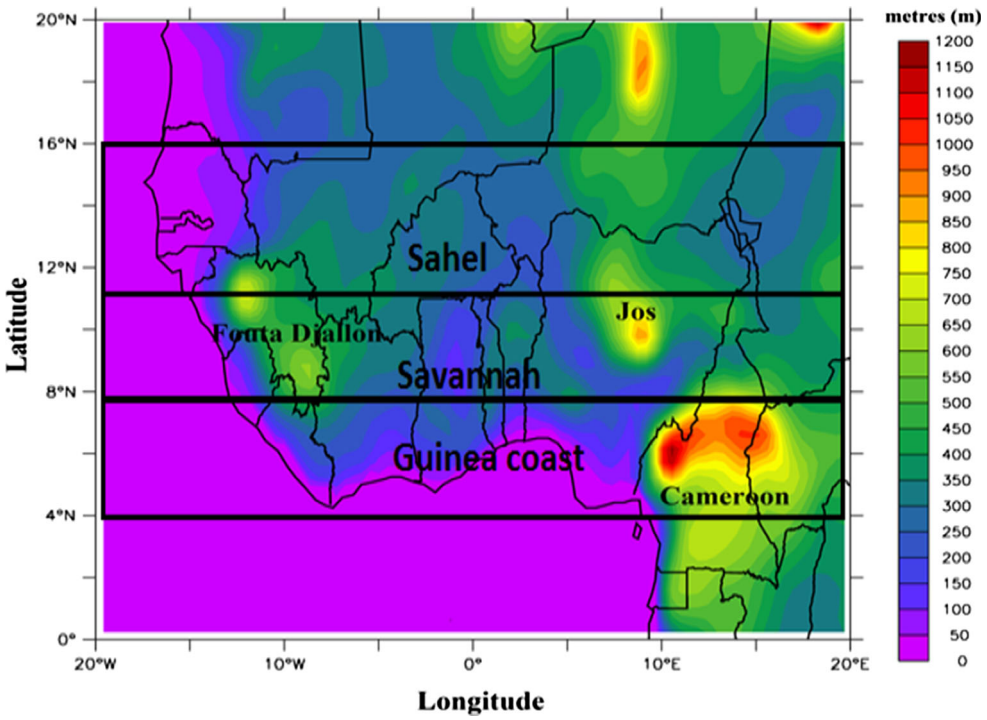

Fig. 1 Study domain showing West Africa topography and the regions designated as Guinea Coast, Savanna, and Sahel zones in the study [Adapted from Akinsanola et al. 2017]

Data and methodology

In this study, an ensemble of seven RCMs participating in the CORDEX-Africa program is analyzed and intercompared (details are presented in Table 1). These RCMs were integrated over Africa continuously for a 20-year period from 1989 to 2008 at a spatial resolution of 50 km (∼0.44°), employing the ERA-Interim reanalysis dataset (Dee et al. 2011) at the lateral boundaries and for initialization. The first year of the simulation run was regarded as spin-up and thus was not included in the analysis. In this study, the simulations were evaluated over the West Africa domain (0°–20°N, 20°W–20°E), which exhibits some localized highlands (Fig. 1). The domain is further subdivided into three climatic zones: Guinea Coast (4°–8°N), Savannah (8°–11°N), and Sahel (11°–16°N). The Guinea Coast represents the southern boundary to the Atlantic Ocean which is characterized by the subhumid climate with an average annual rainfall of 1250–1500 mm. The Savannah zone is a semiarid zone with an average annual rainfall of 750–1250 mm, while the Sahel zone covers the northern boundary of Mauritania, Mali, and Niger. This zone is essentially characterized by a single rainfall peak within a short rainy season (June–September), with an average annual rainfall of about 750 mm.

All the simulation datasets were obtained from the Climate Systems Analysis Group (CSAG) of the University of Cape Town, Cape Town, South Africa. Rainfall data from ground observation, Climate Research Unit (CRU), and Tropical Rainfall Measuring Mission (TRMM) were used to compare and validate the RCMs. The ground observation data were obtained from the African rainfall database of the Institute of Geophysics and Meteorology of the University of Cologne, Germany, for 81 meteorological stations in West Africa covering the period 1990–2008, detail description in (Akinsanola et al. 2015, 2016); the Climate Research Unit (CRU) Time Series (TS) at the University of East Anglia, CRU TS 3.24 (Mitchell and Jones 2005; Harris et al. 2014) is from 1990 to 2008 at 0.5° by 0.5° spatial resolution while the TRMM rainfall was obtained from the Tropical Rainfall Measurement Mission Multi-Platform Analysis (TMPA 3B42V7) (Kummerow et al. 2001; Huffman et al. 2001) at 0.25° by 0.25° spatial resolutions from 1998 to 2008. The 850 hPa wind and specific humidity data used were retrieved from the ERA-Interim reanalysis, a product from European Centre for Medium-range Weather Forecast (ECMWF) at 0.5° by 0.5° spatial resolution from 1990 to 2008.

Since all the products used in this study had different spatial and temporal resolutions, they were first re-gridded to a spatial resolution of ∼0.44° (50 km) using bilinear interpolation as in Nikulin et al. (2012). Also, to address the uniformity in the temporal span of all the dataset, the rainfall data were aggregated into monthly means over the period of 1990–2008. It should be noted that the averaging periods of the TRMM product is necessarily different due to the limited availability periods of the data. However, we assume that this period (i.e., 1998–2008) is informative enough to assess systematic biases, capture year-to-year and seasonal variability, and that the observed differences

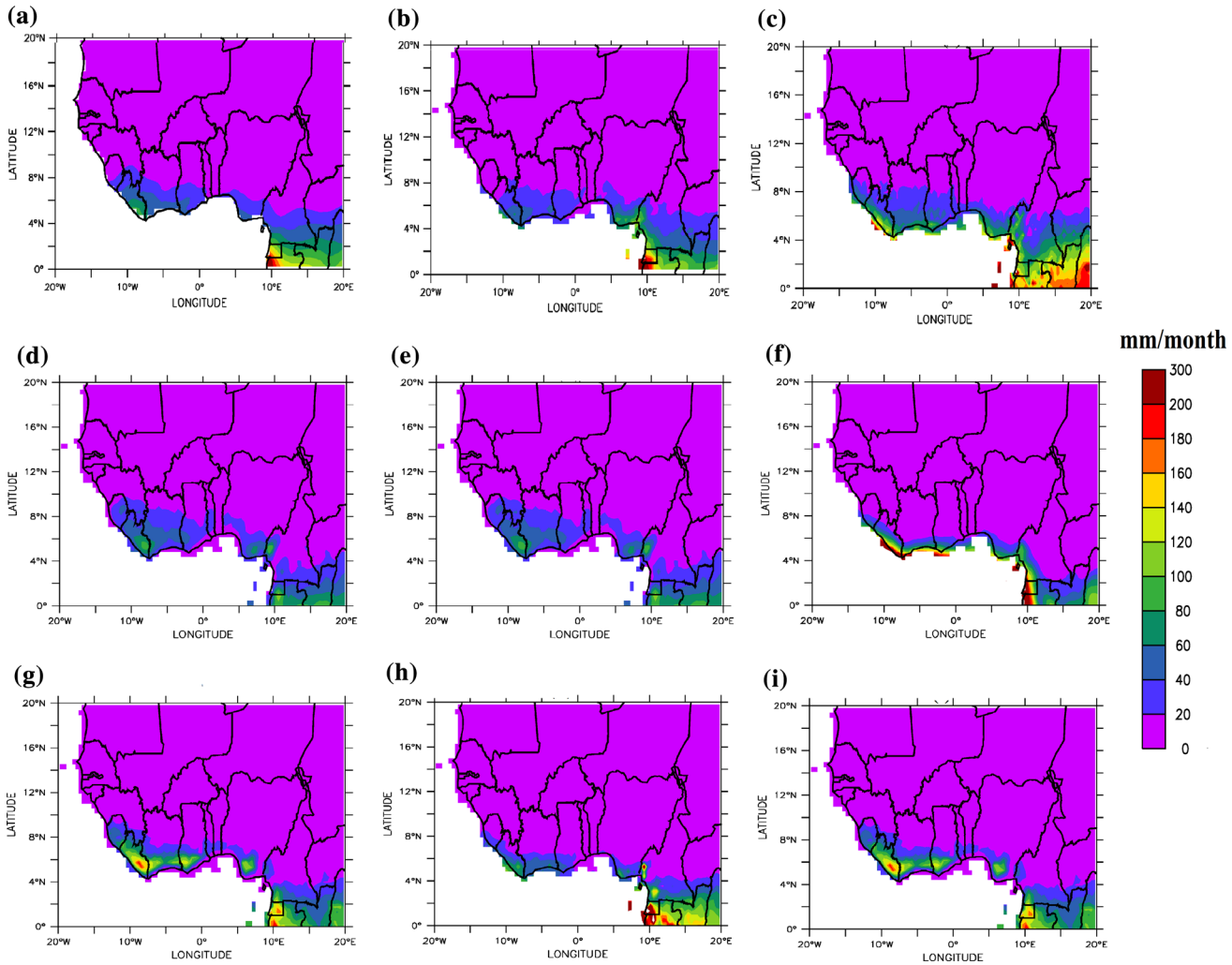

Fig. 2 Spatial pattern of mean monthly DJF rainfall (mm/month) for **a** CRU, **b** TRMM, **c** PRECIS, **d** RCA, **e** REMO, **f** CCLM, **g** CRCM5, **h** HIRHAM, **i** REGCM3 from 1990 to 2008

between the products are dominated by the respective measurement technique rather than long-term climate variability (Hijmans et al. 2005; Akinsanola et al. 2016).

Four seasons were selected to compare and study the rainfall estimates in detail: the dry season (December–February), the pre-rainy season (March–May), the rainy season (June–August), and the post-rainy season (September–November). A comparison was performed for the three main subregions over West Africa. For each subregion and season, the comparison includes a climatological and statistical description. The climatological description is presented by showing the spatial precipitation pattern, latitude–time cross section, interannual and interseasonal variability, the spatial distribution of specific humidity and wind, and lastly, the RCMs depiction of El Nino and La Nina events. For the statistical description, the rainfall simulations of the CORDEX RCMs were assessed using Taylor diagrams (Taylor 2001), which graphically synthesize the degree of correspondence between RCMs and the ground observation in terms of the phase and amplitude of their evolution, measured by Pearson correlation coefficients, the centered root mean square error (RMSE), mean bias error (MBE), and standard deviation (SD). This diagram has been widely used to evaluate the multiple aspects of complex models and gauging the relative skill of many different models (e.g., Kalognomou et al. 2013; Akinsanola et al. 2015).

Furthermore, in order to access extreme events of El Nino and La Nina, the standardized rainfall index was calculated for all the composite years of the two events (the events were sourced from http://ggweather.com/enso/oni.htm). This was done using Eq. 1.

$$\varphi = \frac{x - \bar{x}}{\sigma} \tag{1}$$

where φ represents the standardized rainfall index, x is the actual value of rainfall, $\bar{x}$ is the long-term mean value of

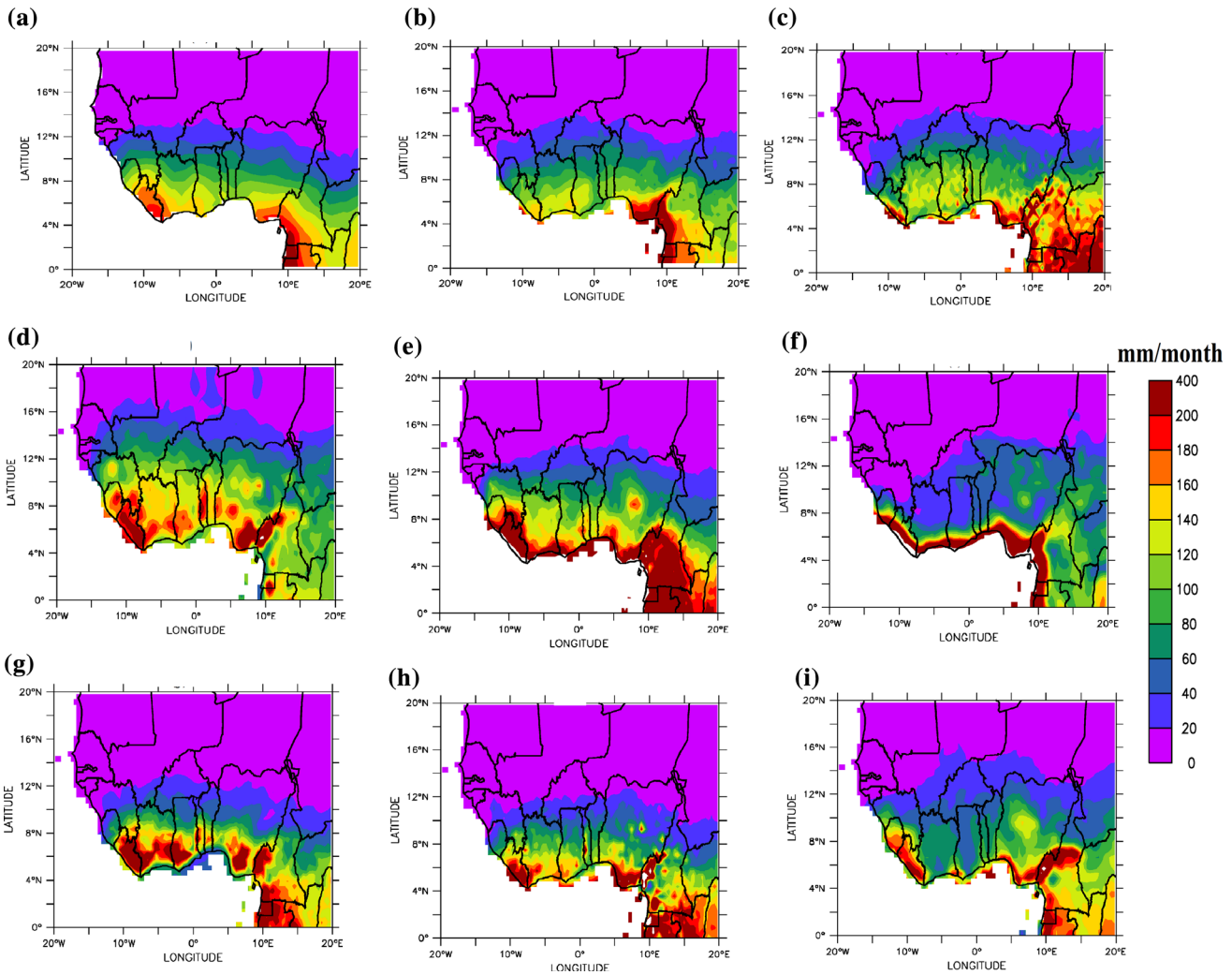

Fig. 3 Spatial pattern of mean monthly MAM rainfall (mm/month) for **a** CRU, **b** TRMM, **c** PRECIS, **d** RCA, **e** REMO, **f** CCLM, **g** CRCM5, **h** HIRHAM, **i** REGCM3 from 1990 to 2008

rainfall, σ is the standard deviation. The dry and wet years have been classified following Mckee et al. (1993).

Results and discussion

Mean climatology

It is very important to assess the abilities and degree at which the RCMs capture the spatial pattern of rainfall over West Africa. Hence, the spatial distribution of the mean December–January–February (DJF) rainfall from (1990 to 2008) over West Africa is shown in Fig. 2a–i for CRU, TRMM, and each of the RCMs used. It was observed that larger portion of West Africa is having rainfall below 20 mm especially north of latitude 8°N. However, rainfall was found to be highest in the eastern part of the Guinea Coast (about longitude 10°E). The RCMs are consistent in capturing the decreasing rainfall from south to north during this period. The pattern obtained for the months of March–April–May (MAM) presented in Fig. 3 is similar to that of DJF. Rainfall amount over the larger part of West Africa is found to have increased reaching the Savannah region (about 11°N), although little or no rainfall is still highly predominant over the Sahel. The zone of highest rainfall is observed to be around the coastal part extending from Liberia toward the southeastern part of Nigeria. This observed region of low and high rainfall amount is consistent in all the datasets, but the amount of rainfall attributed varies to a very large extent from one model to another. Furthermore, the summer June–July–August (JJA) pattern of precipitation as shown in Fig. 4 reveals that rainfall is observed over the entire West Africa domain with the Guinea Coast having the highest rainfall amount. In addition, the zones of maximum rainfall are

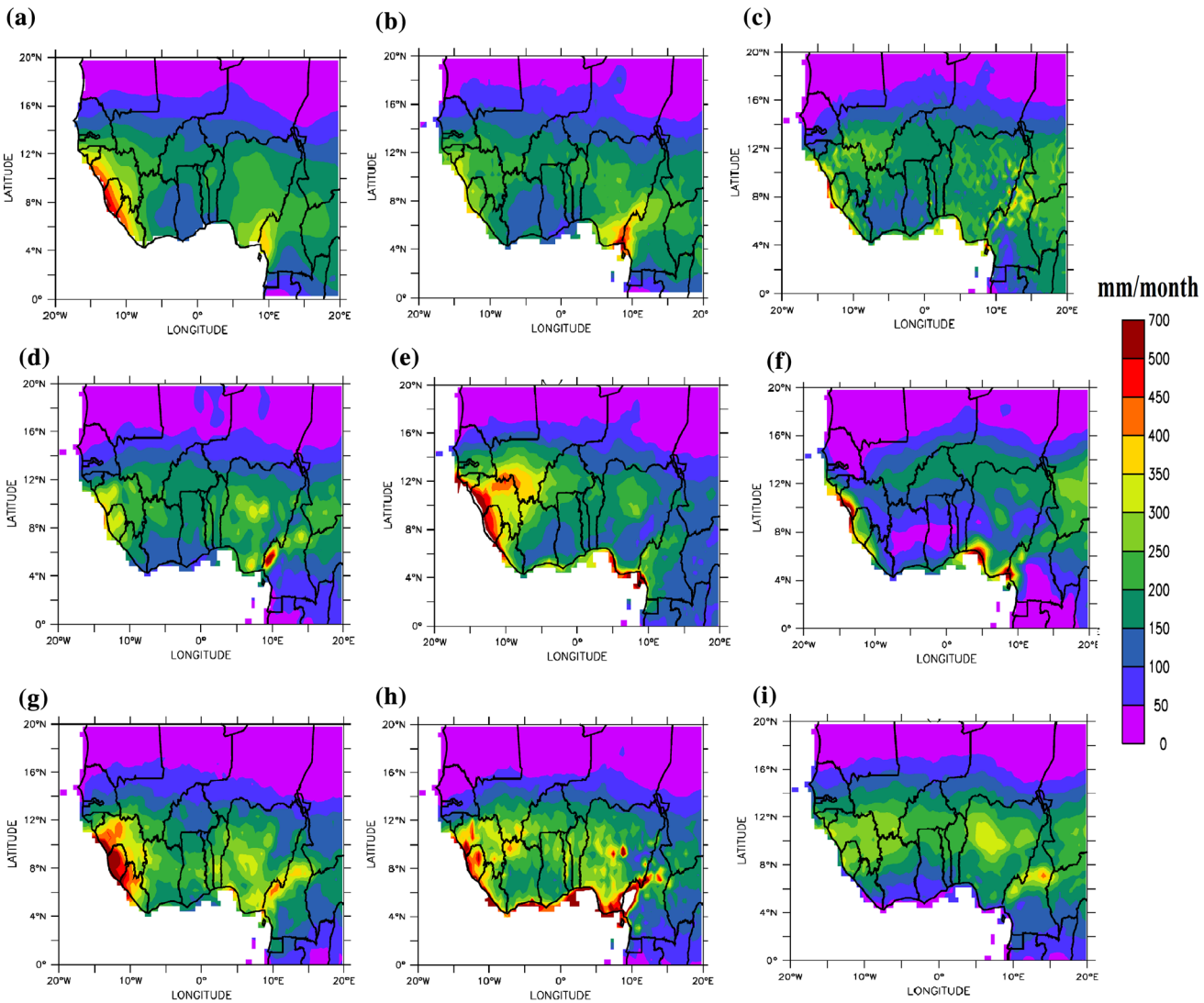

Fig. 4 Spatial pattern of mean monthly JJA rainfall (mm/month) for **a** CRU, **b** TRMM, **c** PRECIS, **d** RCA, **e** REMO, **f** CCLM, **g** CRCM5, **h** HIRHAM, **i** REGCM3 from 1990 to 2008

localized on the major West Africa highlands earlier indicated in Fig. 1. The orography-related rainfall maximum found over the Cameroon Mountains extends from northeast to southwest, with an anvil-like shape encompassing Nigeria and Lake Chad to the left and right, respectively. These observations are well captured by the RCMs. Figure 5 shows the same pattern as Fig. 2 but for the months of September–October–November (SON). The amount of rainfall has reduced drastically compared to that of JJA, although CRCM5 and HIRHAM exhibited a large bias. It can be concluded that rainfall decreases northward as far as the southern fringe of the Sahel region throughout the season. Also, orography plays an important role in West Africa rainfall patterns as reported by Jenkins et al. (2002); Jones et al. (2011); and Akinsanola et al. (2015, 2017). The overestimations of rainfall amount exhibited by some of the models over the highlands may be linked to the model's failure to resolve topography accurately.

Mean annual cycle and Interannual variation

The latitude–time cross section of the mean monthly rainfall over West Africa averaged between longitude 10°W and 10°E is shown in Fig. 6. Here, the ability of the RCMs to capture the three distinctive phases of the WAM (i.e., the onset, the high rain period and the southward retreat) is evaluated. The TRMM data exhibit onset of rainfall around late March and early June, with a progressive extension of the rain belt from the Guinea Coast to about latitude 8°N. Also observed, is a sharp discontinuity known as the monsoon jump as similarly reported in Sultan and Janicot (2000, 2003) and Akinsanola et al. (2015). This jump occurs in the rain band between late June and early

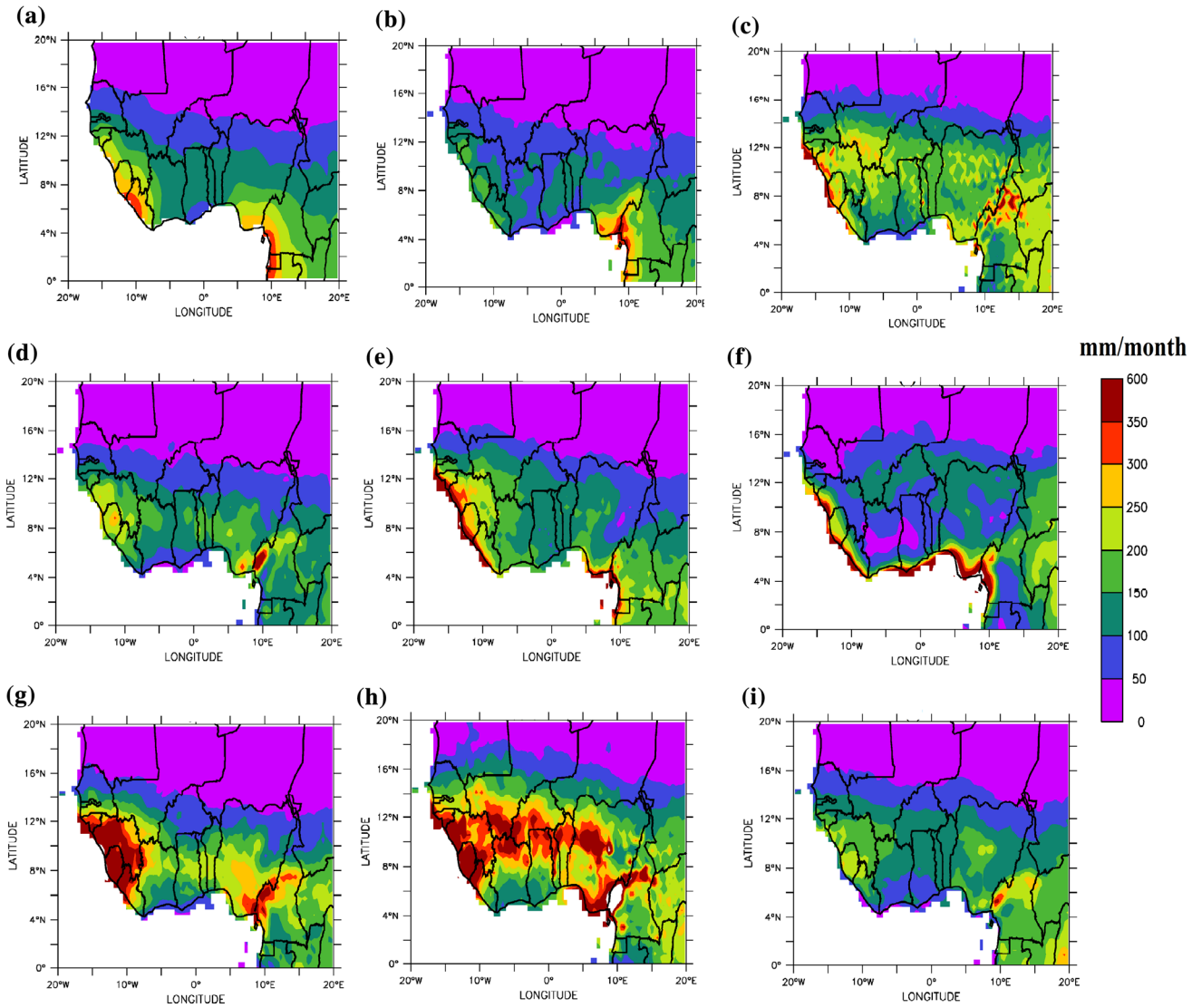

Fig. 5 Spatial pattern of mean monthly SON rainfall (mm/month) for **a** CRU, **b** TRMM, **c** PRECIS, **d** RCA, **e** REMO, **f** CCLM, **g** CRCM5, **h** HIRHAM, **i** REGCM3 from 1990 to 2008

July and is characterized by a northward shift of the monsoon rainfall front to about 10°N. This brings high rainfall amounts into the Sahel accompanied by a sudden cessation in rainfall amount along the Guinea Coast (Gbobaniyi et al. 2013; Akinsanola et al. 2015). Furthermore, around September, the rain band experiences a southward shift toward the Guinea Coast accompanied by a decrease in rainfall amount in the Sahel. The RCMs captured the three distinct phases of the mean annual cycle of the WAM fairly. However, a number of differences were found among the RCMs with regard to the magnitude and spatial extent of the WAM features. For instance, RCA and CRCM5 fail to reproduce the monsoon jump distinctively while CCLM, HIRHAM and REMO largely overestimate the intensity of the pre- and post-monsoon rainfall. It is worth mentioning that most of the deviations and discrepancies occur with respect to the peak of monsoon rainfall over the Sahel. Earlier studies have concluded that divergences in the RCMs annual cycles arise mostly from their different inabilities in simulating the appearance and development of the main features responsible for triggering and maintaining the WAM rainfall. Among them, we have the monsoon flow, AEJ, TEJ, and AEWs (Diallo et al. 2012; Sylla et al. 2013). Therefore, the RCM analyses here may exhibit quite different sensitivities in terms of their response to the intensity of the WAM elements.

The zonal average of the monthly rainfall was evaluated using the ground observation data (81 stations) as reference over the three homogeneous subregions and the entire West Africa domain from 1990 to 2008 as shown in Fig. 7. This

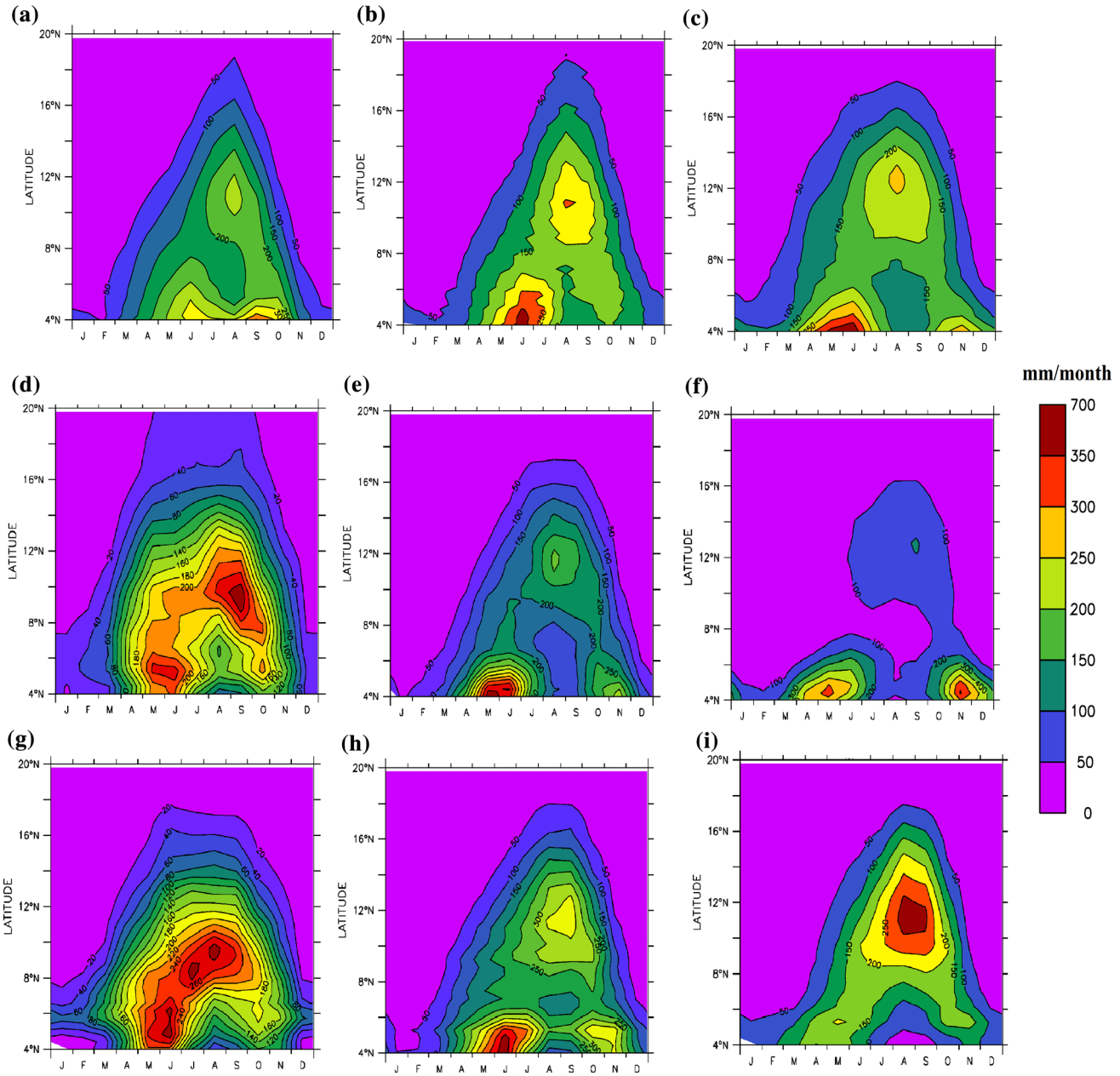

Fig. 6 Latitude–time cross section of mean monthly rainfall (mm/month) for **a** CRU, **b** TRMM, **c** PRECIS, **d** RCA, **e** REMO, **f** CCLM, **g** CRCM5, **h** HIRHAM, **i** REGCM from 1990 to 2008 averaged over longitude 10 W to 10E

helps to better identify rainfall minima and peaks, and thus to further gain insights about the capability of the RCMs in capturing phases and amplitudes during the course of the year in specific homogenous zones. Over the Guinea Coast, the ground observation data exhibited two peaks of rainfall, a primary maximum in June, and a secondary in September. Also present is a relative mid-summer low (minimum) in August known as the little dry season (LDS); this occurs as the monsoon rain band seasonally migrates in the north–south direction in the Guinea Coast. A slight difference was observed in the amount of rainfall among the RCMs, with REMO showing the largest magnitude and REGCM3 the smallest, thus, respectively, overestimating and underestimating the amount of both peaks. It is worth emphasizing that while all the RCMs capture the timing of the mid-summer break, the majority of them simulate an early primary peak in May, but only a few of them shift the secondary maximum to September. These observed differences in the RCM-simulated rainfall may be attributed to their different sensitivities and responses to the prescribed sea surface temperature as reported by Thorncroft et al. (2011). In the Savannah, the length of rainy season

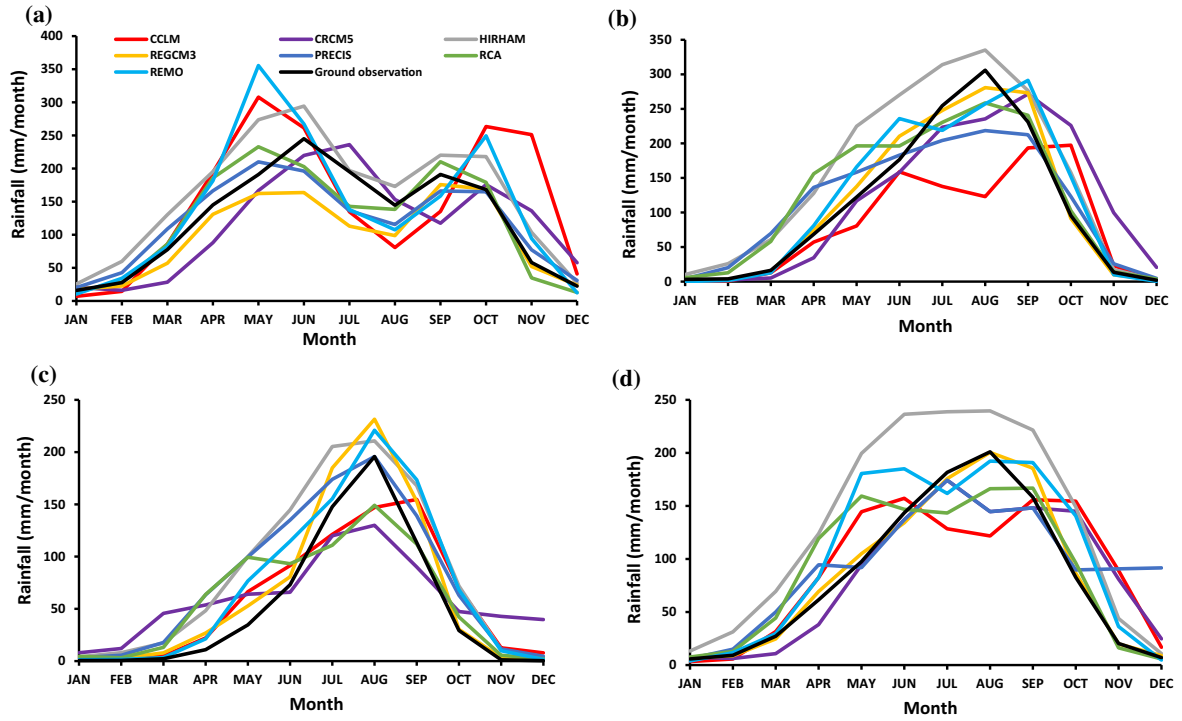

Fig. 7 Zonal variation of mean monthly rainfall (mm/month) for the ground observation and CORDEX RCMs data over **a** Guinea Coast, **b** Savannah, **c** Sahel, and **d** West Africa from 1990 to 2008

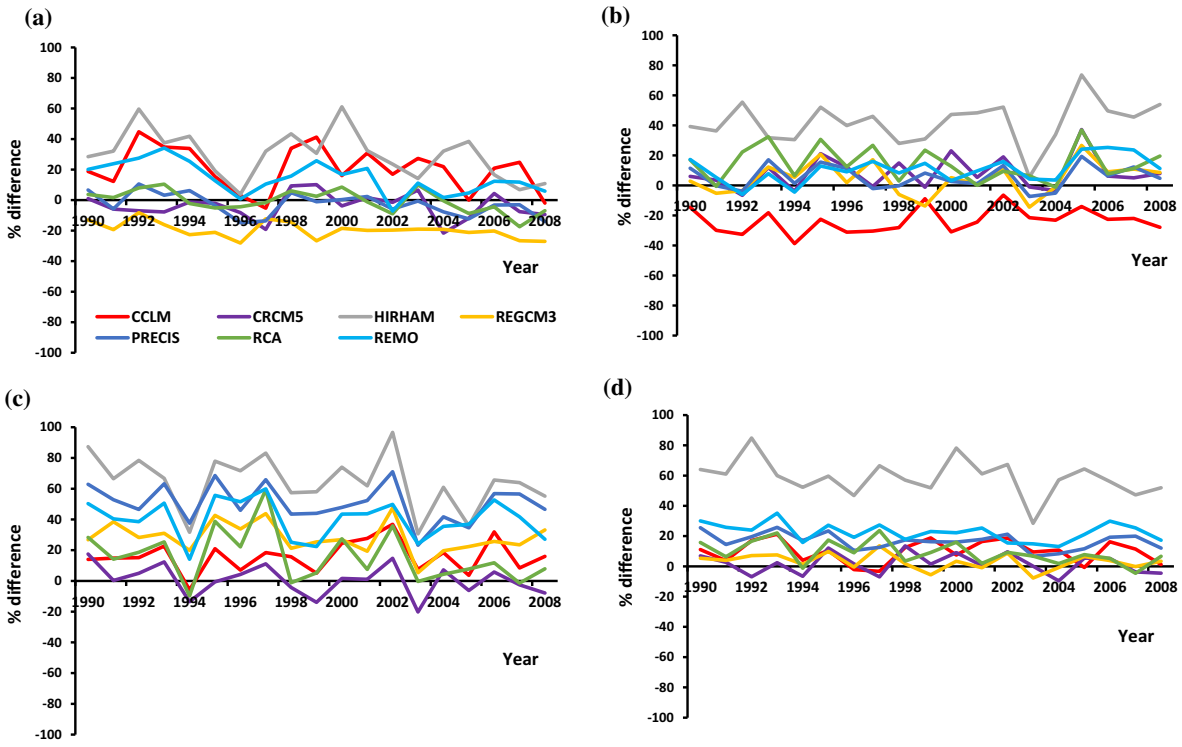

Fig. 8 Inter annual percentage difference of the CORDEX RCMs from ground observation over **a** Guinea Coast **b** Savannah **c** Sahel and **d** whole West Africa from 1990 to 2008

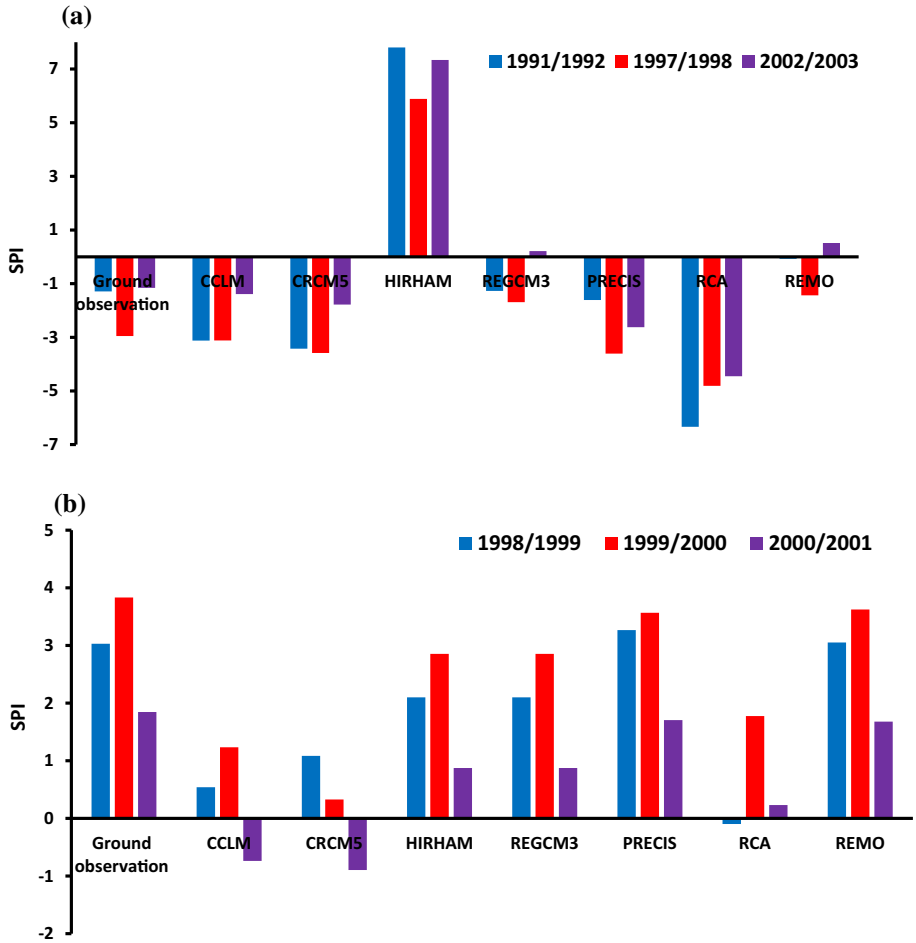

Fig. 9 Standardized rainfall index during JJA for ground observation and CORDEX RCMs associated with **a** El Nino events of 1991/1992, 1997/1998 and 2002/2003 and **b** La Nina events of 1998/1999, 1999/2000, 2000/2001 over West Africa

extends from May to September, rainfall over this region exhibits a unimodal pattern, having its peak in the month of August. Majority of the models captured the observed rainfall distribution but underestimated the rainfall amount during the summer month. HIRHAM was observed to have overestimated rainfall while PRECIS captured two peaks over this zone. In the Sahel, the length of the rainy season is less than four months between July and September, with August having the highest rainfall amount. All the RCMs reproduce the observed rainfall peak in August except CRCM5. REGCM3, HIRHAM, PRECIS, and REMO tend to overestimate its rainfall amount while CRCM5 and RCA considerably underestimated the rainfall amount. In addition, HIRHAM simulates an early peak in July while CCLM shifted the rainfall peak to September. Over the entire West Africa domain, the highest rainfall amount was observed between July and September with a great consistency in all the RCMs.

The percentage difference of the RCMs from the ground observation based on the interannual variation is shown in Fig. 8. The majority of the models depict a large positive difference in the subregions with relatively low deviations over the larger domain of West Africa (about 20%). These indicate that the RCMs have the best performance over a large domain owing to their spatial resolution. The findings presented here are in line with the work of Browne and Sylla (2012), Akinsanola et al. (2017).

Depiction of El Nino and La Nina events

The influence of El Nino–Southern Oscillation (ENSO) on rainfall over West Africa has been evaluated in the previous study (see review in Moron and Ward 1998). Nicholson and Entekhabi (1986), Ropelewski and Halpert (1987, 1989), and Nicholson and Kim (1997) suggest that ENSO influence is minimal, while some others (e.g., Hastenrath 1990; Bhatt 1989; Moron and Ward 1998) suggest that ENSO tends to reduce rainfall in the Sahel. Hence, this study examined rainfall anomalies over West Africa during the summer monsoon months of June–July–August (JJA) associated with El Nino and La Nina events as shown in Fig. 9a and b, using the ground observation data of 81 stations as the reference. Negative anomalies were observed during the El Nino years which implies dry conditions. All the RCMs captured these feature; however, it is worth mentioning that RCA overestimated the event

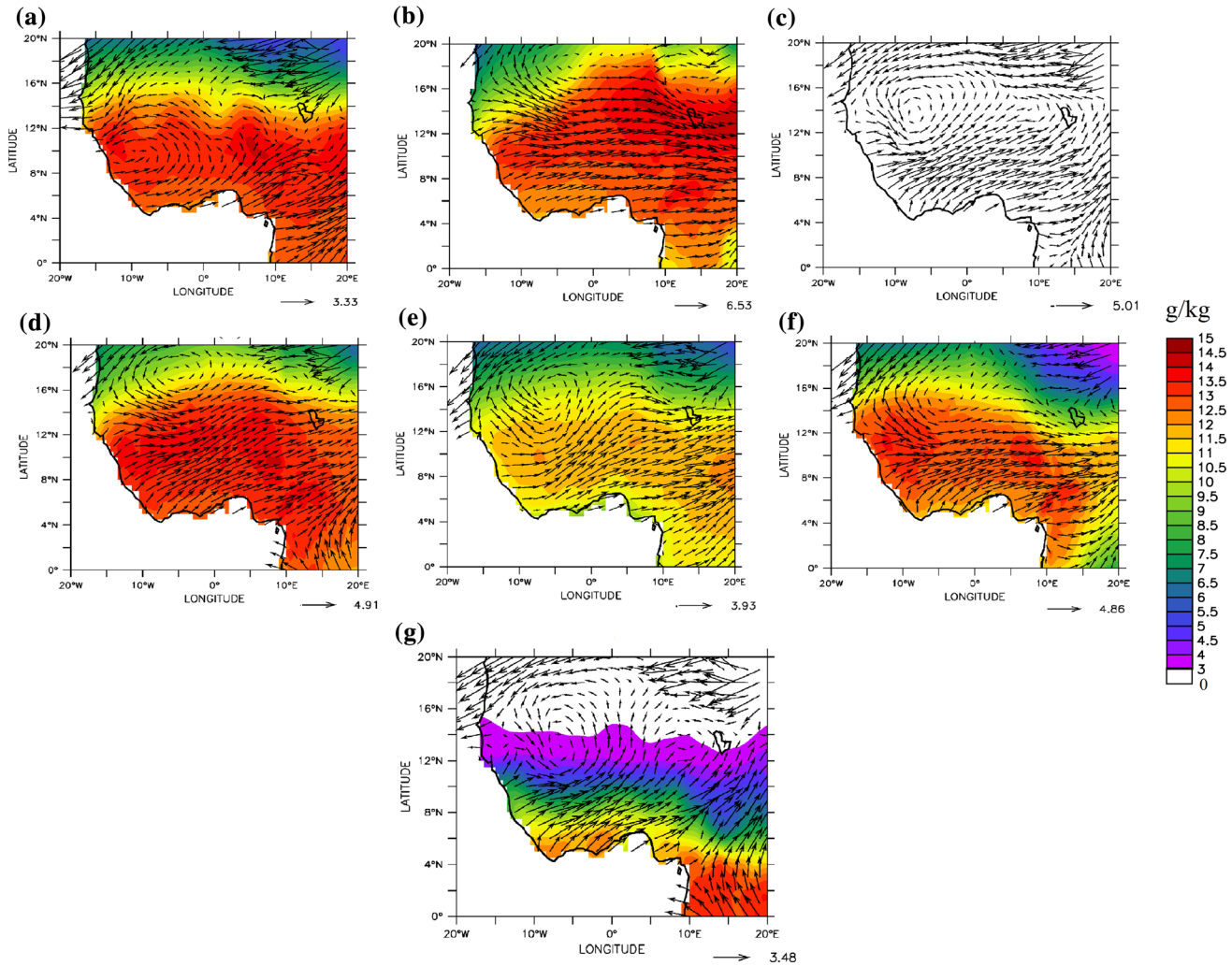

Fig. 10 Spatial distribution of mean JJA 850 hPa specific humidity (g/kg) and wind vector (m/s) for **a** ERA-Interim, **b** CCLM, **c** CRCM5, **d** HIRHAM, **e** REGCM3, **f** RCA, and **g** REMO from 1900 to 2008 over West Africa (*Note: PRECIS data are not available; CRCM5 specific humidity data are also not available*)

while REGCM3, REMO failed to capture the El Nino events of 2002/2003; furthermore, HIRHAM failed to capture the event in all the years (see Fig. 9a). The failure of HIRHAM in capturing the dry conditions associated with El Nino events may be related to rainfall overestimation earlier observed in the model results during summer month. In the La Nina events (see Fig. 9b), positive anomalies were observed implying a wet condition, majority of the RCMs were consistent with the ground observation, although, little underestimation was observed in CCLM and CRCM5. Generally, the two climate events are well captured by the RCMs.

Wind and humidity field

The performance of the model over the West Africa domain requires further examination of the dynamics of the monsoon. Therefore, the wind field and specific humidity distribution at 850 hPa during the summer months of JJA from 1990 to 2008 was investigated and is presented in Fig. 10. The ERA-Interim depicts a narrow band of westerlies located at about 4°N and 8°N, these westerlies propagating from the Atlantic Ocean and extend eastward as far as 20°E, with a maximum westerly flow of 3.33 m/s centered at approximately 12°E over the Cameroon mountains. Similarly, a weak westerly (1 m/s) was observed over the continent and it extends northward to 18°N, overlain by easterlies over the Saharan region. Between latitude 15° and 20°N, two peaks of easterlies are embedded. The first is located between 20° and 10°W with a maximum wind speed of about 5.7 m/s. The second is located between 10° and 20°E and is comparable in magnitude to the first easterlies. The RCM-simulated wind speed is stronger, and

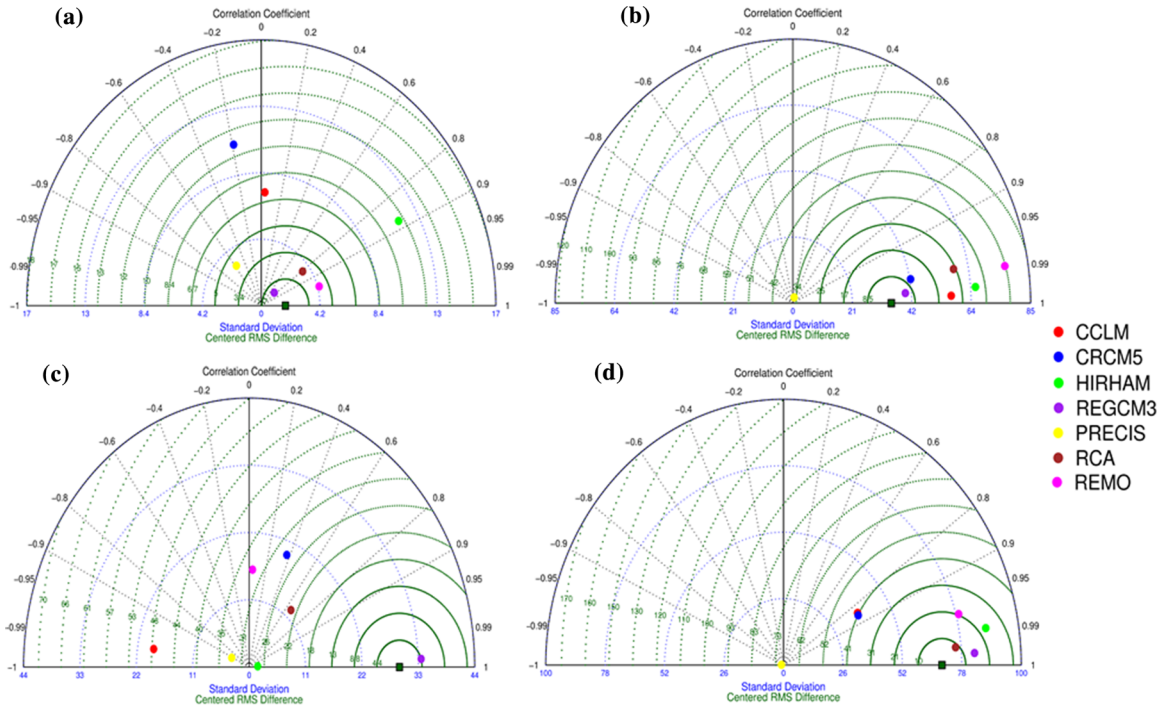

Fig. 11 Taylor diagrams for area-averaged monthly rainfall over Guinea Coast for **a** DJF, **b** MAM, **c** JJA, **d** SON. The reference (ground observation) data are shown by the *green square* along the *horizontal axis*. The individual RCMs are shown by the *solid circles*. The radial coordinate shows the standard deviation. The *azimuthal axis* shows the correlation between the RCMs and the reference data. The centered root mean *square error* is indicated by the *green semicircles* about the reference point

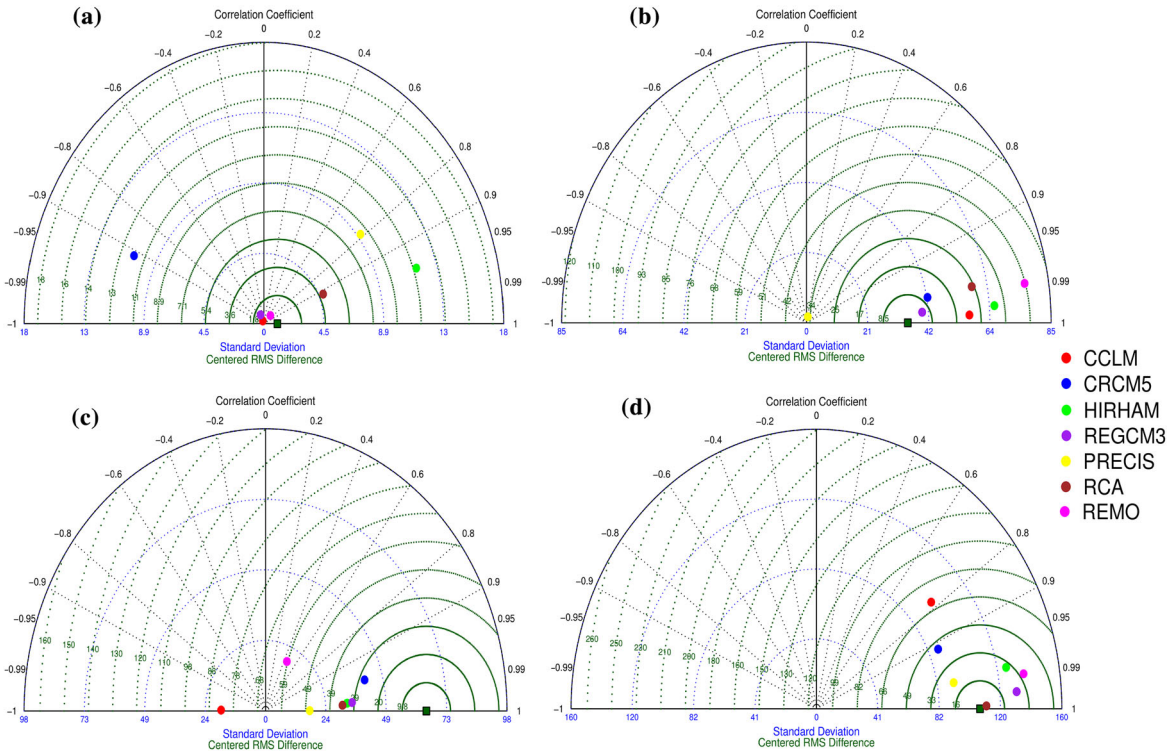

Fig. 12 Taylor diagrams for area-averaged monthly rainfall over Savannah for **a** DJF, **b** MAM, **c** JJA, **d** SON. The reference (ground observation) data are shown by the *green square* along the *horizontal axis*. The individual RCMs are shown by the *solid circles*. The radial coordinate shows the standard deviation. The *azimuthal axis* shows the correlation between the RCMs and the reference data. The centered root mean *square error* is indicated by the *green semicircles* about the reference point

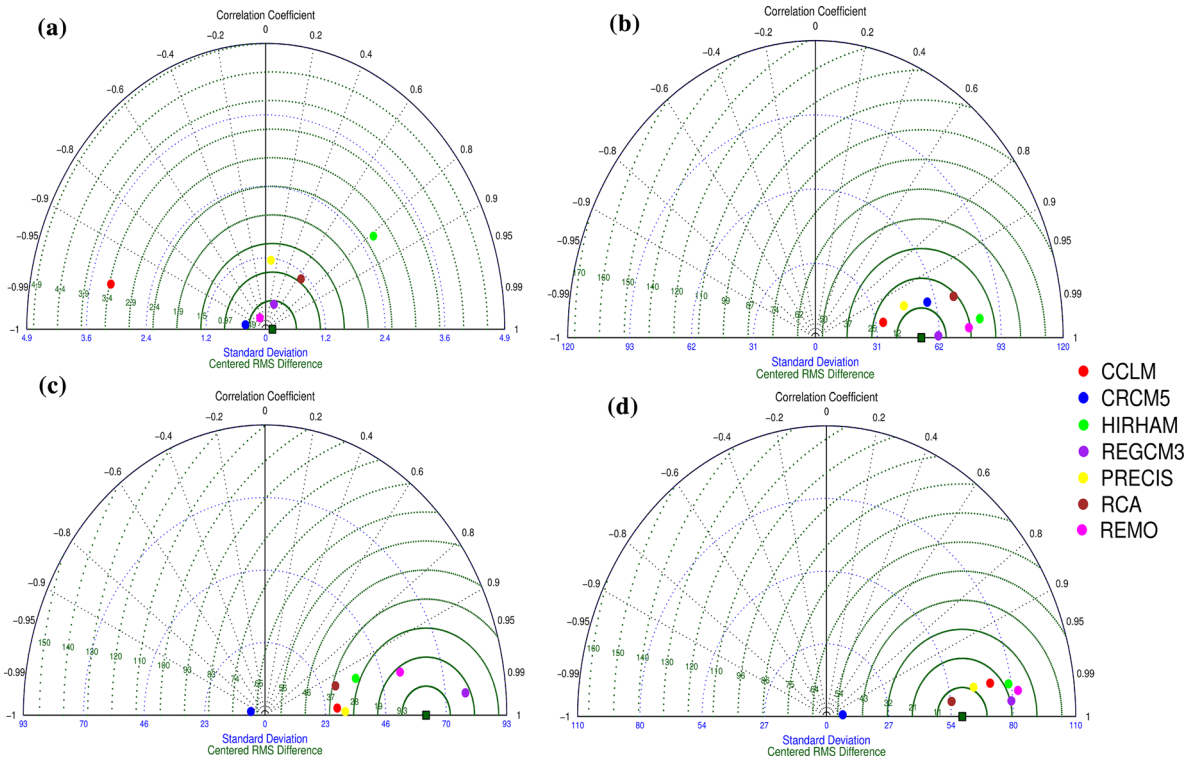

Fig. 13 Taylor diagrams for area-averaged monthly rainfall over Sahel for **a** DJF, **b** MAM, **c** JJA, **d** SON. The reference (ground observation) data are shown by the *green square* along the *horizontal axis*. The individual RCMs are shown by the *solid circles*. The radial coordinate shows the standard deviation. The *azimuthal axis* shows the correlation between the RCMs and the reference data. The centered root mean *square error* is indicated by the *green semicircles* about the reference point

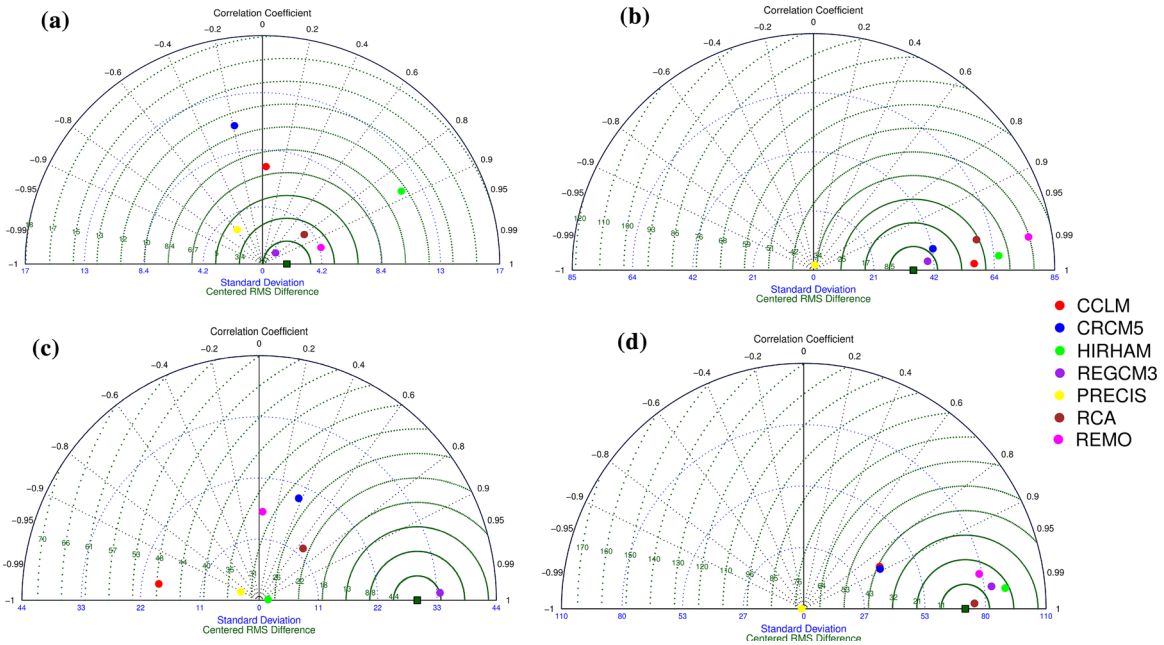

Fig. 14 Taylor diagrams for area-averaged monthly rainfall over the whole West Africa for **a** DJF, **b** MAM, **c** JJA, **d** SON. The reference (ground observation) data are shown by the *green square* along the *horizontal axis*. The individual RCMs are shown by the *solid circles*. The radial coordinate shows the standard deviation. The *azimuthal axis* shows the correlation between the RCMs and the reference data. The centered root mean *square error* is indicated by the *green semicircles* about the reference point

Table 2 Detailed output of the statistical analysis between the RCMs and the ground observation over Guinea Coast and Savannah

Model	MBE	RMSE	*r*	Remarks
Guinea Coast (DJF)				
RCA	**1.38**	**2.46**	**0.81**	**Suitable**
PRECIS	81.06	81.14	−0.58	Not Suitable
CRCM5	5.43	10.37	−0.19	Not Suitable
REMO	**−0.57**	**2.28**	**0.96**	**Suitable**
REGCM3	**0.81**	**1.24**	**0.75**	**Most Suitable**
CCLM	1.29	6.10	0.04	Not Suitable
HIRHAM	**11.08**	**13.62**	**0.88**	**Suitable**
Guinea Coast (MAM)				
RCA	**45.54**	**49.81**	**0.98**	**Suitable**
PRECIS	30.34	41.53	0.24	Not Suitable
CRCM5	**−14.27**	**16.56**	**0.98**	**Suitable**
REMO	**35.52**	**49.48**	**0.99**	**Suitable**
REGCM3	**4.26**	**6.45**	**1.00**	**Most Suitable**
CCLM	**24.12**	**29.83**	**0.65**	**Suitable**
HIRHAM	**68.84**	**73.19**	**0.82**	**Suitable**
Guinea Coast (JJA)				
RCA	**−23.25**	**29.93**	**0.66**	**Suitable**
PRECIS	−84.99	89.09	−0.91	Not Suitable
CRCM5	−23.46	33.07	0.37	Not Suitable
REMO	4.32	27.06	0.04	Not Suitable
REGCM3	**−5.26**	**6.37**	**0.96**	**Most Suitable**
CCLM	−39.57	55.65	−0.99	Not Suitable
HIRHAM	**62.85**	**66.76**	**0.82**	**Suitable**
Guinea Coast (SON)				
RCA	**6.03**	**9.59**	**1.00**	**Most Suitable**
PRECIS	2.68	57.15	−0.99	Not Suitable
CRCM5	**37.64**	**50.56**	**0.86**	**Suitable**
REMO	**35.50**	**39.48**	**0.97**	**Suitable**
REGCM3	**10.28**	**15.95**	**0.98**	**Suitable**
CCLM	**46.08**	**57.44**	**0.85**	**Suitable**
HIRHAM	**51.12**	**54.73**	**0.99**	**Suitable**
Savannah (DJF)				
RCA	**4.37**	**5.40**	**0.92**	**Most Suitable**
PRECIS	**6.52**	**9.47**	**0.79**	**Suitable**
CRCM5	5.28	10.79	−0.91	Not Suitable
REMO	**−2.38**	**2.45**	**0.69**	**Suitable**
REGCM3	−0.90	1.44	−0.41	Not Suitable
CCLM	−2.39	2.56	−0.42	Not Suitable
HIRHAM	**9.90**	**13.34**	**0.96**	**Suitable**
Savannah (MAM)				
RCA	**45.54**	**49.81**	**0.98**	**Suitable**
PRECIS	30.34	41.53	0.24	Not Suitable
CRCM5	**−14.27**	**16.56**	**0.98**	**Suitable**
REMO	**35.52**	**49.48**	**0.99**	**Suitable**
REGCM3	**4.26**	**6.45**	**1.00**	**Most Suitable**
CCLM	**24.12**	**29.83**	**0.78**	**Suitable**
HIRHAM	**68.84**	**73.19**	**0.81**	**Suitable**
Savannah (JJA)				
RCA	**−17.15**	**32.69**	**0.91**	**Suitable**
PRECIS	**−43.67**	**58.29**	**0.84**	**Suitable**
CRCM5	**−39.91**	**45.69**	**0.97**	**Suitable**
REMO	−8.29	48.93	0.45	Not Suitable
REGCM3	**0.69**	**24.70**	**0.92**	**Most Suitable**
CCLM	−105.80	125.73	−1.00	Not Suitable
HIRHAM	**60.78**	**66.26**	**0.79**	**Suitable**
Savannah (SON)				
RCA	**5.82**	**6.93**	**1.00**	**Most Suitable**
PRECIS	**7.18**	**20.48**	**0.99**	**Suitable**
CRCM5	**85.74**	**93.30**	**0.92**	**Suitable**
REMO	**37.81**	**47.78**	**0.99**	**Suitable**
REGCM3	**11.46**	**24.54**	**1.00**	**Suitable**
CCLM	**24.72**	**62.97**	**0.77**	**Suitable**
HIRHAM	**37.17**	**44.53**	**0.98**	**Suitable**

Note best performing models are in bold

Table 3 Detailed output of the statistical analysis between the RCMs and the ground observation over Sahel and West Africa

Model	MBE	RMSE	*r*	REMARKS
Sahel (DJF)				
RCA	**2.79**	**2.91**	**0.64**	**Suitable**
PRECIS	3.99	4.10	0.09	Not Suitable
CRCM5	38.81	38.81	−0.98	Not Suitable
REMO	1.01	1.05	−0.51	Not Suitable
REGCM3	1.73	1.77	0.37	Not Suitable
CCLM	3.58	4.52	−0.97	Not Suitable
HIRHAM	**4.53**	**4.99**	**0.81**	**Most Suitable**
Sahel (MAM)				
RCA	**67.83**	**70.50**	**0.97**	**Suitable**
PRECIS	**52.41**	**53.99**	**0.96**	**Suitable**
CRCM5	**−16.89**	**20.92**	**0.97**	**Suitable**
REMO	**17.51**	**26.29**	**1.00**	**Suitable**
REGCM3	**6.31**	**9.38**	**1.00**	**Most Suitable**
CCLM	**−18.88**	**25.05**	**0.98**	**Suitable**
HIRHAM	**68.78**	**73.06**	**1.00**	**Suitable**
Sahel (JJA)				
RCA	**−21.10**	**36.20**	**0.94**	**Suitable**
PRECIS	**29.35**	**38.78**	**0.92**	**Suitable**
CRCM5	−79.21	96.36	−0.98	Not Suitable
REMO	**24.79**	**28.41**	**0.97**	**Most Suitable**
REGCM3	**26.81**	**30.07**	**0.97**	**Suitable**
CCLM	**−18.94**	**33.73**	**0.95**	**Suitable**
HIRHAM	**48.05**	**53.74**	**0.95**	**Suitable**

Table 3 continued

Model	MBE	RMSE	*r*	REMARKS
Sahel (SON)				
RCA	**5.29**	**7.91**	**0.99**	**Most Suitable**
PRECIS	**23.22**	**25.15**	**0.99**	**Suitable**
CRCM5	**0.98**	**41.95**	**1.00**	**Suitable**
REMO	**35.94**	**41.68**	**0.99**	**Suitable**
REGCM3	**14.25**	**22.89**	**1.00**	**Suitable**
CCLM	**31.26**	**34.27**	**0.99**	**Suitable**
HIRHAM	**35.62**	**40.37**	**0.99**	**Suitable**
West Africa (DJF)				
RCA	**1.38**	**2.46**	**0.81**	**Suitable**
PRECIS	81.06	81.14	−0.58	Not Suitable
CRCM5	5.43	10.37	−0.19	Not Suitable
REMO	**−0.57**	**2.28**	**0.96**	**Suitable**
REGCM3	**0.81**	**1.24**	**0.75**	**Most Suitable**
CCLM	1.29	6.10	0.04	Not Suitable
HIRHAM	**11.08**	**13.62**	**0.88**	**Suitable**
West Africa (MAM)				
RCA	**45.54**	**49.81**	**0.98**	**Suitable**
PRECIS	30.34	41.53	0.24	Not Suitable
CRCM5	**−14.27**	**16.56**	**0.98**	**Suitable**
REMO	**35.52**	**49.48**	**0.99**	**Suitable**
REGCM3	**4.26**	**6.45**	**1.00**	**Most Suitable**
CCLM	**24.12**	**29.83**	**0.72**	**Suitable**
HIRHAM	**68.84**	**73.19**	**0.69**	**Suitable**
West Africa (JJA)				
RCA	**−23.25**	**29.93**	**0.66**	**Suitable**
PRECIS	84.99	−0.91	−0.60	Not Suitable
CRCM5	−23.46	33.07	0.37	Not Suitable
REMO	4.32	27.06	0.04	Not Suitable
REGCM3	**−5.26**	**6.37**	**1.00**	**Most Suitable**
CCLM	−39.57	55.65	−0.99	Not Suitable
HIRHAM	**62.85**	**66.76**	**0.76**	**Suitable**
West Africa (SON)				
RCA	**1.93**	**4.27**	**0.96**	**Most Suitable**
PRECIS	−1.42	58.90	−0.89	Not Suitable
CRCM5	**33.54**	**47.62**	**0.89**	**Suitable**
REMO	**31.40**	**34.12**	**0.98**	**Suitable**
REGCM3	**6.17**	**13.81**	**0.99**	**Suitable**
CCLM	**41.98**	**54.19**	**0.88**	**Suitable**
HIRHAM	**47.02**	**49.72**	**0.99**	**Suitable**

Note best performing models are in bold

the westerly jet spans more latitudes than the ERA-Interim. The observed westerlies in the RCMs extend zonally between latitude 4° and 12°N with local westerly maxima of 6.53 m/s in situ at approximately 12°N. Also, the majority of the RCMs simulates maximum westerly flow at 12°E, but locates it farther north along Lake Chad at 10°N, with a dominance of cyclonic circulation over Mauritania. The observed circulation may imply high moisture convergence and upward motion owing to the presence of high humidity of about 10–15 g/kg, and these may in turn result into heavy rainfall. These observations may be the reason for overestimation earlier observed in the RCMs. Ultimately, the RCMs simulate monsoon that penetrates more northward to about 16°N, covering the lower half of the Sahel. The difference in the northward extent of the monsoon between ERA-Interim and RCMs may be due to the differences in the strength of the simulated westerlies as indicated earlier, in particular, the westerly jet. In fact, studies have shown that the low-level westerly jet is an important agent for moisture transporting from the eastern tropical Atlantic Ocean into continental of West Africa during boreal summer (Patricola and Cook, 2007; Pu and Cook 2010, 2011).

Statistical evaluation

Taylors diagram (Taylor 2001) was employed to assess the models' ability in skillfully simulating rainfall over the three homogeneous subregions and the entire West Africa domain as presented in Figs. 11, 12, 13, 14 and later summarized in Tables 2 and 3. Seasonal means of December–February (DJF), March–May (MAM), June–August (JJA), and September–November (SON) were used for the computation. The results shown are based on the interannual variation of seasonal mean rainfall for the period 1990–2008. Each RCM were compared against the ground observation data using mean bias error (MBE), standard deviation (SD), root mean square error (RMSE) and Pearson's correlation coefficient (r). Over the Guinea Coast (Fig. 11), the RCMs exhibits a remarkable results $r > 0.7$ and having a standard deviation in the vicinity of the ground observation in most of the seasons. PRECIS failed to reproduce the magnitude of the interannual variability in all the seasons while CCLM failed to reproduce the observed rainfall during the DJF and JJA (see Table 2). In the Savannah (Fig. 12), most of the RCMs were able to reproduce the observed rainfall in all the seasons ($r > 0.69$). Although, CCLM exhibited a poor performance during the DJF and JJA seasons while CRCM5 and REGCM3 also failed to reproduce the observed rainfall variability in the DJF seasons. In the Sahel and entire West Africa domain (Figs. 13 and 14 and Table 3), majority of the RCMs exhibited a remarkable performance in all the seasons, except in the Sahel during the DJF season where majority of the model exhibited poor performance. It is evident that the RCMs performance varies from one subregion and season to another, implying that no single

model is best at all time. However, based on individual model performances, REGCM3 consistently outperformed all the other models over the three subregions and the entire West Africa domain in all seasons.

Conclusion

This study has evaluated the ability of seven CORDEX regional climate models (DMI-HIRHAM5, ICTP-REGCM3, CLMcom-CCLM4.8, MPI-REMO, SMHI-RCA35, UCT-PRECIS, and UQAM_CRCM5) in reproducing the rainfall characteristics over West Africa. These models have been evaluated against TRMM and CRU rainfall products, while the ground observation rainfall data from 81 ground observing stations over West Africa have been further employed for comparison and validation. In simulating the spatial rainfall distribution, the overall performance of the RCMs is good, particularly to the north of the study domain. Other aspects of the simulated rainfall that are of practical significance such as the three distinctive stages of the West African monsoon is well captured by some of the RCMs, although with noticeable bias. The significant bias found in some of the RCMs ranges from failure to reproduce the monsoon jump observed in RCA and CRCM5 to considerable overestimation of rainfall amount during pre- and the post-monsoon periods observed in CCLM, HIRHAM, and REMO. Furthermore, the mean annual cycle of rainfall was fairly replicated by the RCMs; this includes the single (double-peaked) rainfall over the Sahel (Guinea Coast). Also, the RCMs reproduce considerably the interannual rainfall variation; the subregions had higher positive bias reaching up to 70% while the larger domain of West Africa exhibited the lowest bias of about 20%. These results imply that the RCMs had the best performance over a larger domain than over the subregions, thus emphasizing the importance of subdividing a large domain such as West Africa into different homogeneous subregions for evaluation analyses. Despite the overall satisfactory performance of the RCMs, it should be emphasized that individual models exhibited noticeable bias, which largely varied in magnitude from one season and subregion to another.

Ultimately, the RCMs largely reproduced the corresponding negative (positive) rainfall anomalies observed during the El Nino (La Nina) years, although RCA overestimated the El Nino events for all the years considered while REGCM3, REMO failed to capture the El Nino events of 2002/2003. The HIRHAM, however, failed to capture all the El Nino events considered. Compared to the ERA-Interim, the RCMs simulated a stronger wind field at 850 hPa and had wider spatial extent of strong westerly wind. In addition, an intense cyclonic circulation and high humidity were observed around Mauritania (11°–17°N, 0°–15°W) in the majority of the models. These observations may be the reason for the earlier reported overestimation in rainfall amount. Lastly, the result of the statistics indicated that the model's performance varied from one subregion to another, as well as from season to season. However, on the basis of individual model performance REGCM3 consistently outperformed all the other models as it captured almost all the basic West Africa rainfall characteristics. Therefore, this study suggests its use for impact studies of climate variability and change over the region.

Acknowledgements The authors appreciate WCRP and START for setting up and funding the CORDEX-Africa analysis initiative and the University of Cape Town for leading the training and analysis program. We are very grateful to regional downscaling groups who kindly shared the downscaled data used in this analysis. We are grateful to the services that have operated the TRMM and CRU and also the African rainfall database of the Institute of Geophysics and Meteorology, University of Cologne, Germany, for the provision of the ground observation data. The efforts of Mr. Abolude Akintayo Temiloluwa and the two anonymous reviewers are also acknowledged.

References

Akinsanola AA, Ogunjobi KO (2015) Recent Homogeneity Analysis and Long Term Spatio-temporal Rainfall Trends in Nigeria. Theor Appl Climatol. doi:10.1007/s00704-015-1701-x

Akinsanola AA, Ogunjobi KO, Gbode IE, Ajayi VO (2015) Assessing the capabilities of three regional climate models over CORDEX Africa in simulating West African summer monsoon precipitation. Adv Meteorol 2015. doi:10.1155/2015/935431

Akinsanola AA, Ogunjobi KO, Ajayi VO, Adefisan EA, Omotosho JA, Sanogo S (2016) Meteorol Atmos Phys. doi:10.1007/s00703-016-0493-6

Akinsanola AA, Ajayi VO, Adejare AT, Adeyeri OE, Gbode IE, Ogunjobi KO, Nikulin G, Abolude AT (2017) Evaluation of rainfall simulations over West Africa in dynamically downscaled CMIP5 global circulation models. Theor Appl Climatol. doi:10.1007/s00704-017-2087-8

Baldauf M, Schulz JP (2004) Prognostic precipitation in the Lokal Modell (LM) of DWD. COSMO Newsletter, No. 4, DWD, Offenbach, Germany, 177–180

Baldauf M, Seifert A, Forstner J, Majewski D, Raschendorfer M, Reinhardt T (2011) Operational convective-scale numerical weather prediction with the COSMO model: description and sensitivities. Mon Weather Rev 139:3887–3905

Benoit R, Cote J, Mailhot J (1989) Inclusion of a TKE boundary layer parameterization in the Canadian regional finite-element model. Mon Weather Rev 117:1726–1750

Bhatt U (1989) Circulation regimes of rainfall anomalies in the Africa-South Asian monsoon belt. J Climate 2:1133–1144

Browne NAK, Sylla MB (2012) Regional climate model sensitivity to domain size for the simulation of the West African monsoon rainfall. Int J Geophys. doi:10.1155/2012/625831

Burpee RW (1972) The origin and structure of easterly waves in the lower troposphere of North Africa. J Atmos Sci 29:77–90

Buzzi M, Rotach MW, Raschendorfer M, Holtslag AAM (2011) Evaluation of the COSMO-SC turbulence scheme in a shear-driven stable boundary layer. Meteor Z 20:335–350

Christensen OB, Drews M, Christensen JH (2006) The HIRHAM regional climate model version 5. DMI Tech. Rep. 06–17, pp 22

Cuxart J, Bougeault Redelsperger JL (2000) A turbulence scheme allowing for mesoscale and large-eddy simulations. Q J R Meteorol Soc 126:1–30

Dee DP et al (2011) The ERA-Interim reanalysis: configuration and performance of the data assimilation system. Q J R Meteorol Soc 137:553–597

Delage Y (1997) Parameterising sub-grid scale vertical transport in atmospheric models under statically stable conditions. Bound Layer Meteorol 82:23–48

Diallo I, Sylla MB, Camara M, Gaye AT (2012) Interannual variability of rainfall and circulation features over the Sahel based on multiple regional climate models simulations. Appl Climatol, Theor. doi:10.1007/s00704-012-0791-y

Diallo I, Sylla MB, Camara M (2013) Gaye AT (2013) Interannual variability of rainfall and circulation features over the Sahel based on multiple regional climate models simulations. Theor Appl Climatol 113(1–2):351–362

Dickinson RE, Henderson-Sellers A, Kennedy PJ (1993) Biosphere-atmosphere transfer scheme (BATS) version 1E as coupled to the NCAR community climate model. NCAR Technical Note NCAR/TN-387+STR. doi:10.5065/D67W6959

Doms G, Forstner J, Heise E, Herzog HJ, Raschendorfer M, Schrodin R, Reinhardt T, Vogel G (2007) A description of the nonhydrostatic regional model LM (version 3.20).Part II: Physical parameterization. Consortium for Small Scale Modelling Rep, p 161

Druyan LM, Feng J, Cook KH, Xue Y, Fulakeza M, Hagos SM, Konaré A, Moufouma-Okia W, Rowell DP, Vizy EK, Ibrah SS (2010) The WAMME regional model intercomparison study. Clim Dyn 35(1):175–192. doi:10.1007/s00382-009-0676-7

Edwards JM, Slingo A (1996) Studies with a flexible new radiation code. I: choosing a configuration for a large-scale model. Q J R Meteorol Soc 122:689–719

Essery RLH, Best MJ, Betts RA, Cox PM (2003) Explicit representation of sub grid heterogeneity in a GCM land surface scheme. J Hydrometeor 4:530–543

Fink AH, Reiner A (2003) Spatiotemporal variability of the relation between African easterly waves and West African squall lines in 1998 and 1999. J Geophys Res 108(D11):4332. doi:10.1029/2002JD002816

Fink AH, Vincent DG, Ermert V (2006) Rainfall types in the West African Sudanian zone during the summer monsoon 2002. Mon Weather Rev 134:2143–2164

Flato G, Marotzke J, Abiodun B, Braconnot P, Chou S, Collins W, Cox P, Driouech F, Emori S, Eyring V, Forest C, Glecker P, Guilyardi E, Jacob C, Kattsov V, Reason C, Rummukainen M (2013) Evaluation of Climate Models, in: Climate Change: The Physical Science Basis. Contribution of Working Group I to the Fifth Assessment Report of the Intergovernmental Panel on Climate Change, Cambridge University Press, Cambridge, United Kingdom and New York, NY, USA

Fouquart Y, Bonnel B (1980) Computations of solar heating of the earth's atmosphere: a new parameterization. Beitr Phys Atmos 53:35–62

Fritsch JM, Chappell CF (1980) Numerical prediction of convectively driven mesoscale pressure systems. Part I: convective parameterization. J Atmos Sci 37:1722–1733

Gbobaniyi E, Sarr A, Sylla MB, Diallo I, Lennard C, Dosio A, Dhiediou Kamga A, Klutse NAB, Hewitson B, Nikulin G, Lamptey B (2013) Climatology, annual cycle and interannual variability of precipitation and temperature in CORDEX simulations over West Africa. Int J Climatol 34:2241–2257. doi:10.1002/joc.3834

Giannini A, Saravanan R, Chang P (2003) Oceanic forcing of Sahel rainfall on interannual to interdecadal timescales. Science 302:1027–1030

Giorgetta M, Wild M (1995) The water vapour continuum and its representation in ECHAM4. MPI Rep. 162, p 38

Giorgi F, Jones C, Asrar GR (2009) Addressing climate information needs at the regional level: the CORDEX framework. World Meteorol Org Bull 58:175

Gregory D, Allen S (1991) The effect of convective downdraughts upon NWP and climate simulations. In: 9th Conference on Numerical Weather Prediction, Denver, CO, American Meteorological Society pp 122–123

Gregory D, Rowntree PR (1990) A mass flux convection scheme with representation of cloud ensemble characteristics and stability-dependent closure. Mon Weather Rev 118:1483–1506

Grell GA (1993) Prognostic evaluation of assumptions used by cumulus parameterizations. Mon Weather Rev 121:764–787

Hagemann S (2002) An improved land surface parameter dataset for global and regional climate models. MPI Rep. 336, p 21

Harris I, Jones PD, Osborn TJ, Lister DH (2014) Updated high resolution grids of monthly climatic observations—the CRU TS3.10 dataset. Int J Clim 34:623–642. doi:10.1002/joc.3711

Hastenrath S (1990) The relationship of highly reflective clouds to tropical climate anomalies. J. Climate 3:353–365

Herzog HJ, Vogel G, Schubert U (2002) LLM–a nonhydrostatic model applied to high-resolving simulations of turbulent fluxes over heterogeneous terrain. Theor Appl Climatol 73:67–86

Hijmans RJ, Cameron SE, Parra JL, Jones PG, Jarvis A (2005) Very high resolution interpolated climate surfaces for global land areas. Int J Climatol 25(15):1965–1978

Holtslag AAM, de Bruijn EIF, Pan HL (1990) A high resolution air mass transformation model for short-range weather forecasting. Mon Weather Rev 118:1561–1575

Huffman GJ, Adler RF et al (2001) Global precipitation at one-degree daily resolution from multisatellite observations. J Hydrometeorol 2(1):36–50

Jacob D (2001) A note to the simulation of the annual and interannual variability of the water budget over the Baltic Sea drainage basin. Meteorol Atmos Phys 77:61–73

Jacob D, Barring L, Christensen OB, Christensen JH, de Castro M, Deque M, Giorgi F, Hagemann S, Hirschi M, Jones R, Kjellstrom E, Lenderink G, Rockel B, Sanchez E, Schar C, Seneviratne SI, Somot S, van Ulden A, van den Hurk B (2007) An inter-comparison of regional climate models for Europe: model performance in present day climate. Clim Change 81:31–52

Jenkins GS, Kamga A, Garba A, Diedhiou A, Morris V, Joseph E (2002) Investigating the West African climate system using global/regional climate models. Bull Am Meteorol Soc 83:583–595

Jones RG, Noguer M, Hassel D, Hudson D, Wilson S, Jenkins G, Mitchell J (2004) Generating high resolution climate change scenarios using PRECIS. Met Office Hadley Centre Handbook, p 40. [Available online at http://www.metoffice.gov.uk/media/pdf/6/5/PRECIS_Handbook.pdf.]

Jones C, Giorgi F, Asrar G (2011) The coordinated regional downscaling experiment: CORDEX an international downscaling link to CMIP5CLIVAR Exchanges 16: pp 34–39

Jung G, Kunstmann H (2007) High-resolution regional climate modeling for the Volta region of West Africa. J Geophys Res 112:D23108. doi:10.1029/2006JD007951

Kain JS, Fritsch JM (1990) A one-dimensional entraining/detraining plume model and its application in convective parameterization. J Atmos Sci 47:2784–2802

Kain JS, Fritsch JM (1993) Convective parameterization for mesoscale models: the Kain–Fritsch scheme. The Representation of Cumulus Convection in Numerical Models, Meteor. Monogr. No. 46, Am Meteorol Soc pp 165–170

Kalognomou EA, Lennard C, Shongwe M, Pinto I, Favre A, Kent M, Hewitson B, Dosio A, Nikulin G, Panitz H-J, Büchner M (2013) A diagnostic evaluation of precipitation in CORDEX models over southern Africa. J Clim 26:9477–9506

Kiehl JT, Hack JJ, Bonan GB, Boville BA, Briegleb BP, Williamson DL, Rasch PJ (1996) Description of the NCAR Community Climate Model (CCM3). NCAR Tech. Note NCAR/TN-4201STR, p 152

Kim J, Waliser DE, Mattmann C, Goodale C, Hart A, Zimdars P, Crichton D, Jones C, Nikulin G, Hewitson B, Jack C, Lennard C, Favre A (2014) Evaluation of the CORDEX-Africa multi-RCM hindcast: systematic model errors. Clim Dyn 42:1189–1202

Kummerow C, Hong Y, Olson WS, Yang S, Adler RF, McCollum J, Ferraro R, Petty G, Shin DB, Wilheit TT (2001) The evolution of the Goddard profiling algorithm (GPROF) for rainfall estimation from passive microwave sensors. J Appl Met 40:1801–1840

Kuo HL (1965) On formation and intensification of tropical cyclones through latent heat release by cumulus convection. J Atmos Sci 22:40–63

Le Barbe L, Lebel T, Tapsoba D (2002) Rainfall variability in West Africa during the years 1950–90. J Clim 15(2):187–202

Li J, Barker HW (2005) A radiation algorithm with correlated-k distribution. Part I: local thermal equilibrium. J Atmos Sci 62:286–309

Lohmann U, Roeckner E (1996) Design and performance of a new cloud microphysics scheme developed for the ECHAM general circulation model. Clim Dyn 12:557–572

Louis JF (1979) A parametric model of vertical eddy fluxes in the atmosphere. Bound Layer Meteorol 17:187–202

Lu J, Delworth TL (2005) Ocean forcing of the late 20th century Sahel drought. Geophys Res Lett 32:L22706. doi:10.1029/2005GL023316

McKee TB, Doesken NJ, Kleist J (1993) The relationship of drought frequency and duration of time scales. In: 8th Conference on Applied Climatology, American Meteorological Society, Jan 17–23, 1993, Anaheim CA, pp 179–186

Mlawer EJ, Taubman SJ, Brown PD, Iacono MJ, Clough SA (1997) Radiative transfer for inhomogeneous atmospheres: RRTM, a validated correlated-k model for the longwave. J. Geophys. Res, 102 (D14), 16 663–16 682

Morcrette JJ, Smith L, Fouquart Y (1986) Pressure and temperature dependence of the absorption in long wave radiation parameterizations. Beitr Phys Atmos 59:455–469

Moron V, Ward MN (1998) ENSO teleconnections with climate variability in the European and African sectors. Weather 53:287–295

Nicholson SE, Entekhabi D (1986) The quasi –periodic behavior of rainfall variability in Africa and its relationship to the southern oscillation. Arch Meteorol Geophys Bio Klimatol series A 34:311–348

Nicholson SE, Kim J (1997) The relationship of the El Niño-southern oscillation to African rainfall. Int J Climatol 17:117–135

Nikulin G, Jones C, Giorgi F, Asrar G, Buchner M, Cerezo-Mota R, Christensen OB, Deque M, Fernandez J, Hansler A, van Meijgaard E, Samuelsson P, Sylla MB, Sushama L (2012) Precipitation climatology in an ensemble of CORDEX-Africa regional climate simulations. J Climate 25(18):6057–6078

Omotosho JB, Abiodun BJ (2007) A numerical study of moisture build-up and rainfall over West Africa. Meteorol Appl 14:209–225

Paeth H, Hall NM, Gaertner MA, Alonso MD, Moumouni S, Polcher J, Ruti PM, Fink AH, Gosset M, Lebel T, Gaye AT, Rowell DP, Moufouma-Okia W, Jacob D, Rockel B, Giorgi F, Rummukainen M (2011) Progress in regional downscaling of west African precipitation. Atmos Sci Lett 12(1):75–82. doi:10.1002/asl306

Pal JS, Small EE, Eltahir EAB (2000) Simulation of regional-scale water and energy budgets: representation of subgrid cloud and precipitation processes within RegCM. J Geophys Res 105(D24):29 579–29 594

Pal JS et al (2007) Regional climate modeling for the developing world: the ICTP RegCM3 and RegCNET. Bull Am Meteorol Soc 88:1395–1409

Parry ML, Canziani OF, Palutikof JP, van der Linden PJ, Hanson CE (2007) Impacts Adaptation and Vulnerability Contribution of Working Group II to the Fourth Assessment Report of the Intergovernmental Panel on Climate Change Cambridge University Press Cambridge UK 2007

Patricola CM, Cook KH (2007) Dynamics of the West African monsoon under mid-Holocene processional forcing: regional climate model simulations. J Clim 20:694–716

Pu B, Cook KH (2010) Dynamics of the West African westerly jet. J Clim 23:6263–6276

Pu B, Cook KH (2011) Role of the West African Westerly jet in Sahel rainfall variations. J Clim. doi:10.1175/JCLI-D-11-00394.1

Rasch PJ, Kristjansson JE (1998) A comparison of the CCM3 model climate using diagnosed and predicted condensate parameterizations. J Clim 11:1587–1614

Rechid D, Raddatz TJ, Jacob D (2009) Parameterization of snow-free land surface albedo as a function of vegetation phenology based on MODIS data and applied in climate modelling. Theor Appl Climatol 95:245–255

Redelsperger JL, Diongue A, Diedhiou A, Ceron JP, Diop M, Gueremy JF, Lafore JP (2002) Multiscale description of a Sahelian synoptic weather system representative of the West African monsoon. Q J R Meteorol Soc 128:1229–1257

Redelsperger JL, Thorncroft CD, Diedhiou A, Lebel T, Parker DJ, Polcher J (2006) African monsoon multidisciplinary analysis: an international research project and field campaign. Bull Am Meteorol Soc 87(12):1739–1746. doi:10.1175/BAMS-87-12-1739

Ritter B, Geleyn JF (1992) A comprehensive radiation scheme of numerical weather prediction with potential application to climate simulations. Mon Weather Rev 120:303–325

Rockel B, Will A, Hense A (2008) The regional climate model COSMO-CLM (CCLM). Meteorol Z 17:347–348

Ropelewski CF, Halpert MS (1987) Global and regional scale precipitation patterns associated with the El Niño/Southern Oscillation. Mon Weather Rev 115:1606–1626

Ropelewski CF, Halpert MS (1989) Precipitation pattern associated with the high index phase of the southern oscillation. J Clim 2:268–284

Rummukainen M (2010) State-of-the-art with regional climate models. Wiley Interdiscip Rev Clim Change 1:82–96. doi:10.1002/wcc8

Samuelsson P, Gollvik S, Ullerstig A (2006) The land-surface scheme of the Rossby Centre regional atmospheric climate model (RCA3).SMHI Rep. Met. 122, p 25

Samuelsson P, Jones CG, Willen U, Ullerstig A, Gollvik S, Hansson U, Jansson C, Kjellstrom E, Nikulin G, Wyser K (2011) The Rossby Centre Regional Climate model RCA3: model description and performance. Tellus 63A:4–23

Sass BH, Rontu L, Savijarvi H, Raisanen P (1994) HIRLAM-2 radiation scheme: Documentation and tests. SMHI HIRLAM Tech. Rep. 16, p 43

Savijarvi H (1990) A fast radiation scheme for mesoscale model and short-range forecast models. J Appl Meteorol 29:437–447

Schulz JP, Dumenil L, Polcher J, Schlosser CA, Xue Y (1998) Land surface energy and moisture fluxes: comparing three models. J Appl Meteorol 37:288–307

Smith RNB (1990) A scheme for predicting layer clouds and their water content in a general circulation model. Q J R Meteorol Soc 116:435–460

Sultan B, Janicot S (2000) Abrupt shift of the ITCZ over West Africa and intraseasonal variability. Geophys Res Lett 27:3353–3356

Sultan B, Janicot S (2003) The West African monsoon dynamics Part II: The "pre-onset" and "onset" of the summer monsoon. J Clim 16:3407–3427

Sundqvist H, Berge E, Kristjansson JE (1989) Condensation and cloud parameterization studies with a mesoscale numerical weather prediction model. Mon Weather Rev 117:1641–1657

Sylla MB, Diallo I, Pal JS (2013) West African monsoon in state-of the-art regional climate models In Climate Variability—Regional and Thematic Patterns Tarhule A (ed) ISBN: 980-953-307-816-3

Taylor KE (2001) Summarizing multiple aspects of model performance in a single diagram. J Geophys Res 106(D7):7183–7192

Thorncroft CD, Nguyen H, Zhang C, Peyrille P (2011) Annual cycle of the West African monsoon: regional circulations and associated water vapour transport. Q J R Meteorol Soc 137(654):129–147

Tiedtke M (1989) A comprehensive mass flux scheme for cumulus parameterization in large-scale models. Mon Weather Rev 117:1779–1800

Tompkins AM (2002) A prognostic parameterization for the sub grid scale variability of water vapor and clouds in large-scale models and its use to diagnose cloud cover. J Atmos Sci 59:1917–1942

Verseghy DL (2000) The Canadian Land Surface Scheme (CLASS): its history and future. Atmos Ocean 38:1–13

Vizy EK, Cook KH (2001) Mechanisms by which Gulf of Guinea and eastern North Atlantic sea surface temperature anomalies influence African rainfall. J Clim 14:795–821

Vizy EK, Cook KH (2002) Development and application of a mesoscale climate model for the tropics: influence of sea surface temperature anomalies on the West African monsoon. J Geophys Res 107(D3):4023. doi:10.1029/2001JD000686

Zadra A, Caya D, Cote J, Dugas B, Jones C, Laprise R, Winger K, Caron LP (2008) The next Canadian Regional Climate Model. Phys Can 64:75–83